BAS

Sensor Notes

Note 3

November 1980

Carbon-Manganin Gage Development

Neal Baum
University of New Mexico
Albuquerque, NM 87131

Abstract

An experimental study of the behavior of a fully active Wheatstone bridge whose elements were carbon and manganin gages was undertaken in order to determine the feasibility of using this gage in a uniaxial flow environment on an underground test. The gage was tested quite successfully on the 4-in gas gun at the Air Force Weapons Laboratory Impact Facility. Peak pressures in these tests reached 20 kbars. The gage was also tested for survivability at 10-kbar stress levels using high explosives. In these tests the gage functioned well for early times; the diagnostic equipment did not function properly for late times.

CONTENTS

ILLUSTRATIONS

TABLES

I. INTRODUCTION

The measurement of stress (or, equivalently, pressure) in a hydrodynamic uniaxial strain environment generated in an underground test has always presented problems to the experimenter. The problems presented are not only those associated with shock-survival time but also those associated with high electrical and radiation-induced noise. The University of New Mexico Engineering Research Institute (NMERI), under contract to the Air Force Weapons Laboratory (AFWL), undertook to determine if a gage could be built to measure stress on an underground test.

The primary gage element chosen for the effort was carbon. The gage requirements were taken from HYBLA GOLD predictions of stress in tunnel walls,* neutron radiation intensity, and the electromagnetic pulse (EMP) (Ref. 1). The basic stress range was 1 to 10 kbars. The limits of the carbon gage go much beyond these limits, and it is felt that the carbon gage is much better than the presently used gages for the stress range indicated.

The presently utilized gages and stress ranges are as follows: quartz, up to approximately 5 kbars; ytterbium, used for the range of 1 to 20 kbars with a maximum possible of 39.4 kbars; and manganin, which has a useful or potential range much higher than 100 kbars.

The limits of stress for the carbon gage are 1 and 100 kbars. These are practical limitations. The 1-kbar lower limit was chosen because normal earth materials are not hydrodynamic in nature at lower stresses. This limit is probably high for some earth material but is definitely low for some others such as granite. Thus, gages utilized for this low-pressure region must be designed to take the effect of arching into account and must be placed so that even minor geological perturbations will not significantly affect their output. This is not to say that the carbon gage is incapable of performing in this region but rather that the approach to measuring stress in this low region is very different from that encountered when the surrounding geology can be assumed to behave as an ideal fluid. Despite the author's feeling that the sensitivity of the carbon gage (with an appropriate design) lends itself to the measurement of this lower stress, it is beyond the scope of this report

---

1. *HYBLA GOLD Radiation Environment Progress Report*, SAI-77-700-LJ, Science Applications, Inc., La Jolla, California, June 1977.

*Private communication to the author from Major Marvin Alme of AFWL/NTY.

to advocate its use in this region because of the variance of the approach that would have to be used. The upper limit was arbitrarily chosen because of the sensitivity reduction of the gage at high stresses. The gage can function to stresses at least 50 percent greater than this, but the gage sensitivity is down to that of manganin at 100 kbars and continues to decrease.

Carbon stress gages have been developed for DNA by EG&G* (Ref. 2), Effects Technology, Inc. (ETI, Ref. 3), and Stanford Research Institute (Ref. 4). These gages were developed to measure shock pressure induced in different materials by radiation deposition. The advantages of the use of carbon for this application are obvious. They are as follows:

1. Low Z: A small radiation cross section is necessary to insure accuracy and survival in a high-radiation environment.

2. Rise time: The short-duration, fast rise-time pulse mandates that the gage itself have a frequency response capable of following the shock profile to the required precision. The carbon gage is capable of resolving 20-ns rise times (Ref. 5). This rise time is dependent upon the material used to encapsulate the gage and upon the gage thickness. The method of gage manufacture is conducive to producing a thin gage.

3. Low temperature coefficient: The heating caused by radiation deposition requires the gage to have a low temperature coefficient. As examples, the Dynasen gage (Ref. 5) (formerly made by EG&G) has a temperature coefficient of -0.0009 Ω/Ω/°C, and ETI's has a temperature sensitivity of ±200 p/m/°C maximum (Ref. 6).

---

2. Charest, J.A., *Development of a Carbon Shock-Pressure Gage*, DNA-3101F, Defense Nuclear Agency, Washington, D.C., 31 July 1973.

3. Naumann, W., *Carbon Stress Gage Development*, Final Report DNA-3027F, Defense Nuclear Agency, Washington, D.C., April 1973.

4. Ginsberg, M.J., DeCarli, P.S., and Dempster, J., *Minute Gun Series* (U), *Diamond Sculls Event* (U), *Carbon Gage Measurements* (U), a confidential report POR 6724, Defense Nuclear Agency, Washington, D.C., 10 October 1973.

5. *Carbon Shock Pressure Gages*, Data Sheet No. 2, brochure from Dynasen, Inc., Goleta, California.

6. *Specification, Carbon Stress Gage*, Effects Technology, Inc., Santa Barbara, California, 14 July 1972.

*EG&G no longer manufactures this gage. The technology was turned over to Dynasen, Inc., of Goleta, California.

4. Low impedance: The ability to transmit fast rise-time signals over long signal cables mandates impedance matching. The carbon gage can be manufactured to have the desired resistance, commonly 50Ω.

5. High signal-to-noise ratio: In this respect, carbon has been shown to perform twice as well as the alternatively used back-surface quartz gage (Ref. 7).

6. Low hysteresis: Gas gun tests at Lawrence Livermore Laboratory have shown that a Dynasen Kapton®-encapsulated carbon gage follows the theoretical shock wave profile (both loading and unloading) in a manner more satisfactory than manganin.* These tests were performed at peak shock levels up to 20 kbars.

Now that some of the properties of the gage have been elucidated, one may compare them with those of the presently utilized stress gages. These gages are quartz, ytterbium, and manganin.

1. Quartz: The quartz gage is a piezoelectric crystal gage used in the charge mode.** The basic disadvantage of this type of gage is its extremely high impedance (10^9 to $10^{13}\Omega$). This impedance makes it difficult to utilize in a field situation because of the electrical leakage that can develop unless extreme care is taken. The hardened form of the gage has been tested successfully up to a peak stress of 5 kbars. It failed when a 10-kbar peak stress was applied.† On the other hand, the low-impedance (usually 50Ω) carbon gage has been calibrated to 150 kbars in gas guns and with magnetic flyer plates.

2. Ytterbium: The ytterbium gage is a piezoresistive gage used between 1 and 20 kbars with practical upper limit of 39.4 kbars. At this upper limit, ytterbium undergoes a polymorphic transformation (faced-centered cubic to

---

7. Steele, E.J., and Naumann, W.J., *Minute Gun Series* (U), *Diamond Sculls Event* (U), *Carbon Gage Evaluation in Diamond Sculls* (U), an S-RD report, POR 6730, Defense Nuclear Agency, Washington, D.C., 10 October 1973.

*Private communication to the author from B. Isbell of Lawrence Livermore Laboratory, Livermore, California.

**As opposed to the back-surface quartz gage used in the current mode.

†Private communication to the author from D. Grine of Systems, Science, and Software, La Jolla, California, February 8, 1974.

body-centered cubic) (Ref. 8). The primary advantage of the gage is its sensitivity. Figure 1 shows that the ytterbium is 3 to 4 times more sensitive than carbon to stress; at first glance one can see why it is used at lower stresses. However, Figure 2 (from Ref. 9) shows the prime difficulty associated with the gage, namely, the hysteresis. In other words, the ytterbium gage unloads in a manner different from the way in which it loads. As indicated in Figure 2, the magnitude of this hysteresis can be significant.

As pointed out previously, the carbon gage exhibits little hysteresis. Thus, it may be concluded that, in spite of the fact that the ytterbium gage is a better voltage modulator, the carbon gage is a better stress gage.

3. Manganin: Manganin is also utilized as a piezoresistive shock gage in the indicated stress range. It clearly has the advantage of extended range

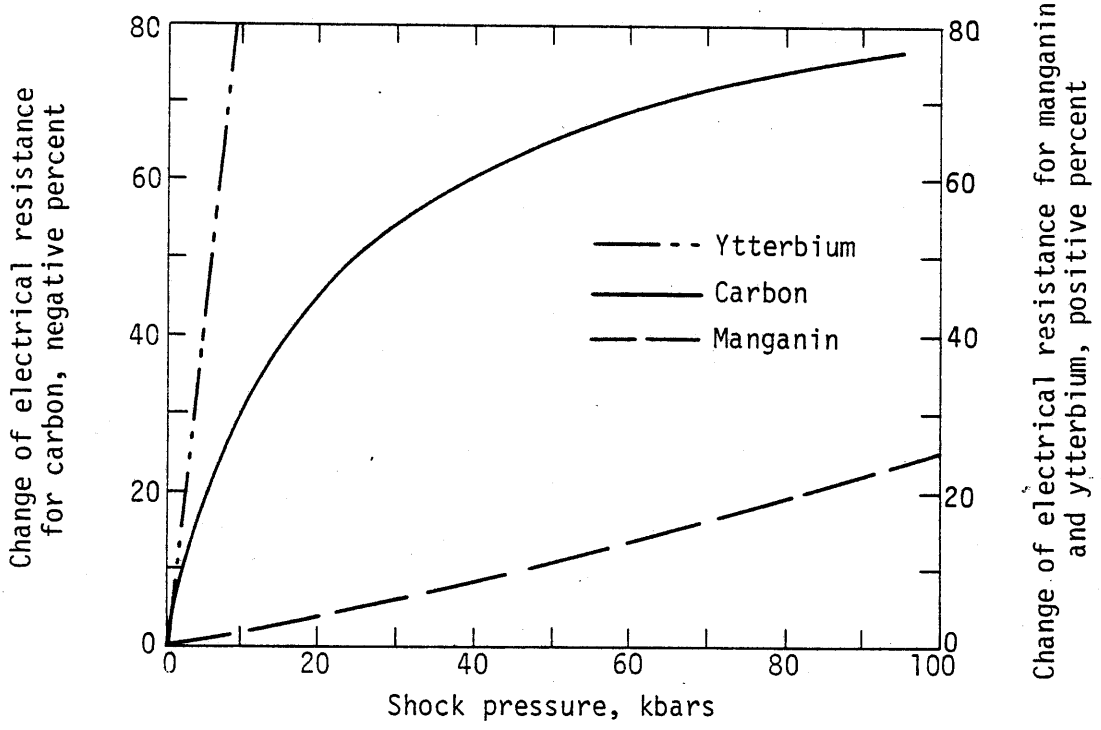

Figure 1. Shock pressure sensitivity of some piezoresistive gages.

8. Ginsberg, M.J., *Calibration and Characterization of Ytterbium Stress Transducers*, DNA-2742F, Defense Nuclear Agency, Washington, D.C., October 1971.

9. Smith, C.W., et al., *Constitutive Relations from In Situ Lagrangian Measurements of Stress and Particle Velocity*, DNA-28831, Defense Nuclear Agency, Washington, D.C., January 1972.

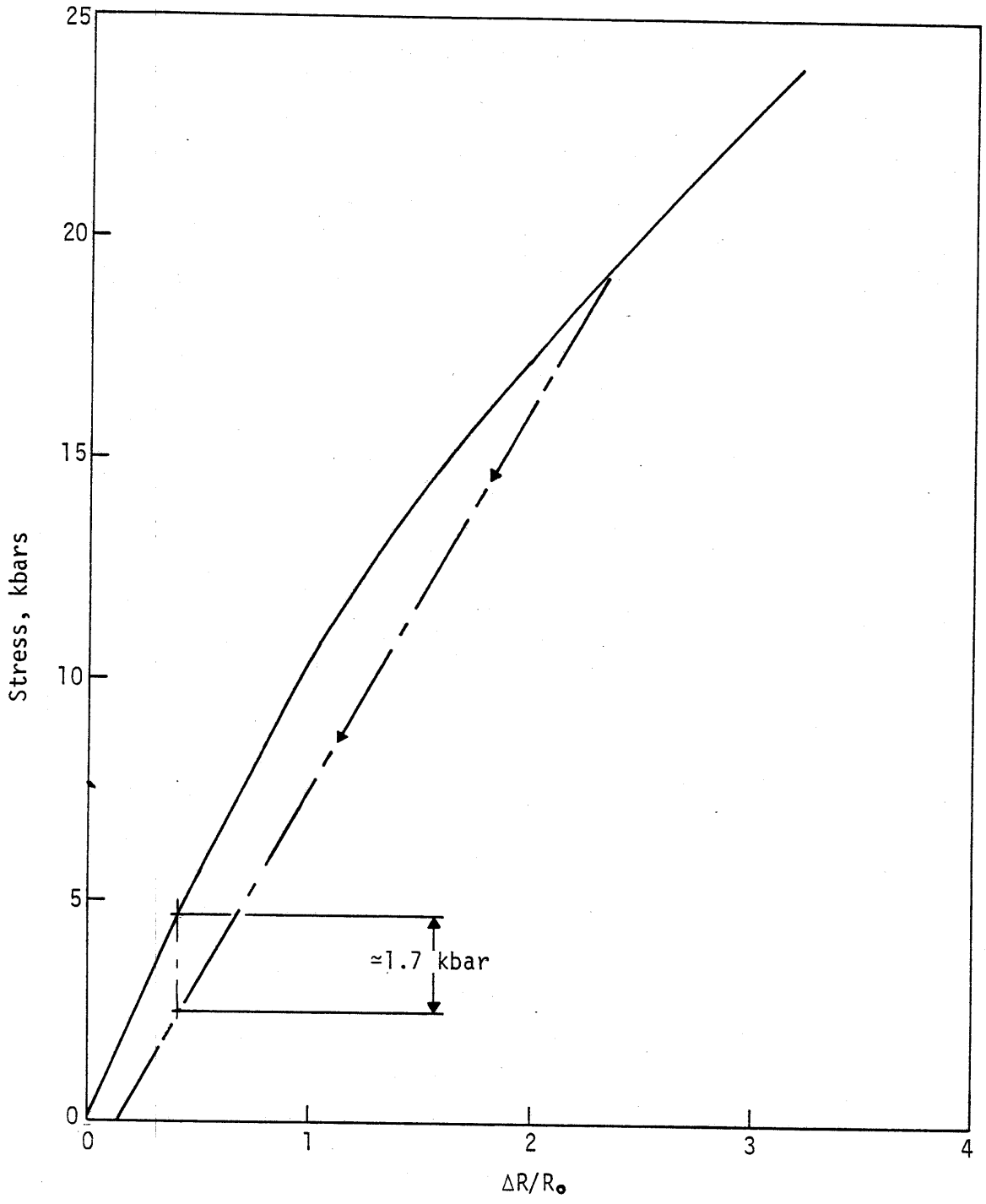

Figure 2. Ytterbium calibration data with one unloading path (Ref. 9).

over carbon; it has been used up to 1 Mbar. On the other hand, one can easily infer from Figure 1 that the carbon gage is much more sensitive in the range of stress below 100 kbars. Since they are both usually 50Ω gages, it may be concluded that the signal-to-noise ratio will be significantly better for the carbon gage.

All piezoresistive gages mentioned in this section (carbon, ytterbium, and manganin) are sensitive to strain. The magnitude of this strain sensitivity is approximately equal for all of these gages; they each have a strain gage factor of about 2. Thus, the gage will have to be designed to insure that shock input of the gage represents, as closely as possible, a uniaxial strain condition. In this manner, the effects of gage stretching are limited.

In review, the specific advantages, in the range of 1 to 100 kbars, of the carbon gage with respect to the presently used gages are the following:

Quartz -- Carbon has a low impedance that can be used at much higher pressures.

Ytterbium -- Carbon does not exhibit the hysteresis that ytterbium does; it also has a more extended range.

Manganin -- In the stress range indicated, carbon is much more sensitive.

The carbon-manganin gage was developed more for electrical reasons than for shock sensitivity. The gage design is that of a fully active Wheatstone bridge. A Wheatstone bridge is simply an array of four resistors as shown in Figure 3. If $\frac{M}{C} = \frac{C'}{M'}$ then the bridge is said to be in balance since the voltage at point a will equal the voltage at point b, and thus there will be no signal (V'). If the C and C' are carbon gages and the M and M' are manganin gages, then, when the gages are subjected to shock pressure, the bridge will become unbalanced and a signal will be produced at the balance point. If the reader will refer to Figure 1, the reader will note that the carbon has a negative sensitivity and manganin has a positive coefficient. The gage thus has an enhanced sensitivity. However, this enhanced sensitivity was not the reason for using manganin since the enhancement is not that great (~10 percent). The desire was to obtain a gage leg that was well characterized from the standpoints of electrical properties change and mechanical survivability. Manganin was chosen to be the other active element because it is probably the most well-characterized material under shock pressure. The characterization is the result of its extensive use over the years.

The existence of an even number of elements gives rise to the possibility of introducing symmetry in the placement of the individual elements in the

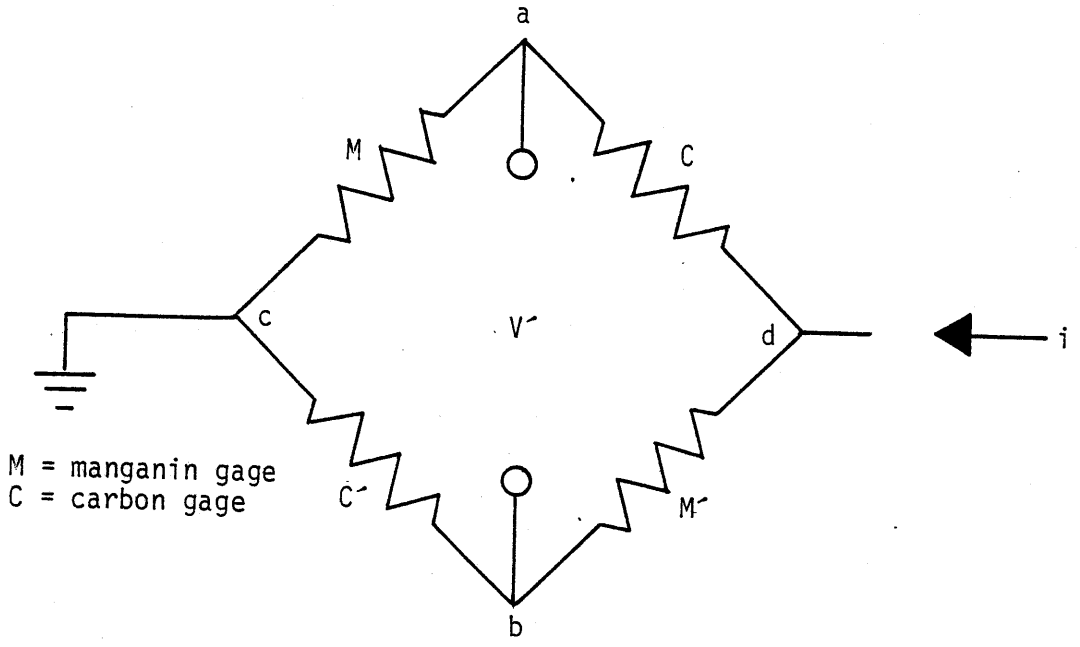

Figure 3. Wheatstone bridge.

bridge, which was impossible when there was a single element in the bridge. Thus the bridge output can be made relatively insensitive to external electromagnetic fields because these components can be made to cancel.

In the past tunnel test (HYBLA GOLD), in which gages were exposed to a relatively mild EMP environment, it was apparent that the principal problem was not the mechanical survivability but rather the noise induced into the output of the gages. Thus it is apparent that care must also be taken with the shielding topology (Ref. 10) and the topology of the conductors and the gages. The topologies should be such that the gage signals are relatively insensitive to the EMP. It was for this reason that the full active bridge was chosen.

Thus it was decided to attempt to develop a fully active bridge gage composed of both carbon and manganin. The primary purpose of this development was to have a gage capable of working in the expected severe shock and electrical noise environment.

---

10. Baum, N., *Topological Concepts as Applied to Electrical Signal Isolation and Mechanical Cable Survivability*, BAS Instrumentation Notes, Note 1 Feb 1980, Air Force Weapons Laboratory, Kirtland AFB New Mexico

II. THE ELECTRICAL TOPOLOGY AND SIGNAL CONDITIONING

The electrical topology is shown in Figure 4. This figure shows Balun transformers that were made under special order to NMERI's specifications by EG&G. They had a 50Ω input impedance, and each one had two 25Ω output connections. The cable used was specially ordered from Uniform Tube and was a 25Ω solid aluminum jacket cable. For some of the experiments, two parallel RG58 cables were used in lieu of the 25Ω cable. This was done because of the expense involved. The excitation and signal cables were RG213.

The Balun transformers were chosen because of their common-mode rejection properties. In other words, if, because of symmetry, it can be presumed that a signal picked up on one of the cables is equal to that picked up on the other, then they will cancel at the center top ground of the Balun.

It should also be noted that the shield is continuous over the whole sensor and that the gage was designed to be impedance-matched with the rest of the system (Section IV).

The excitation was in all cases a Tektronix Model 180A time-mark generator. This generator supplied a continuous sinusoidal 10-MHz wave. The signal output was recorded on scopes. It was then demodulated and recorded on tape. Various demodulators were tried; they were designed to full-wave rectify the narrow band, filtered (±200 kHz), 10-MHz signal. However, none were found to be dependable for normal operation. A 10-MHz WWV radio receiver was then tried in the later tests. The signal was attenuated (30 times) and fed into the antenna; then the output of the receiver was recorded. This too was found to be unsatisfactory because the frequency response, although not empirically determined, was obviously not good enough.

The bridge circuit can be approximated as shown in Figure 5. The following three simultaneous equations can be written using Kirchhoff's laws:

$$
\begin{aligned}
V &= I_1(R_4 + R_1) - I_2R_4 - I_3(R_1 + R_4) \\
0 &= -I_1R_4 + I_2(R_4 + R_3 + R_5) + I_3(R_4 + R_3) \\
0 &= -I_1(R_1 + R_4) + I_2(R_3 + R_4) + I_3(R_1 + R_2 + R_3 + R_4)
\end{aligned}
\qquad (1)
$$

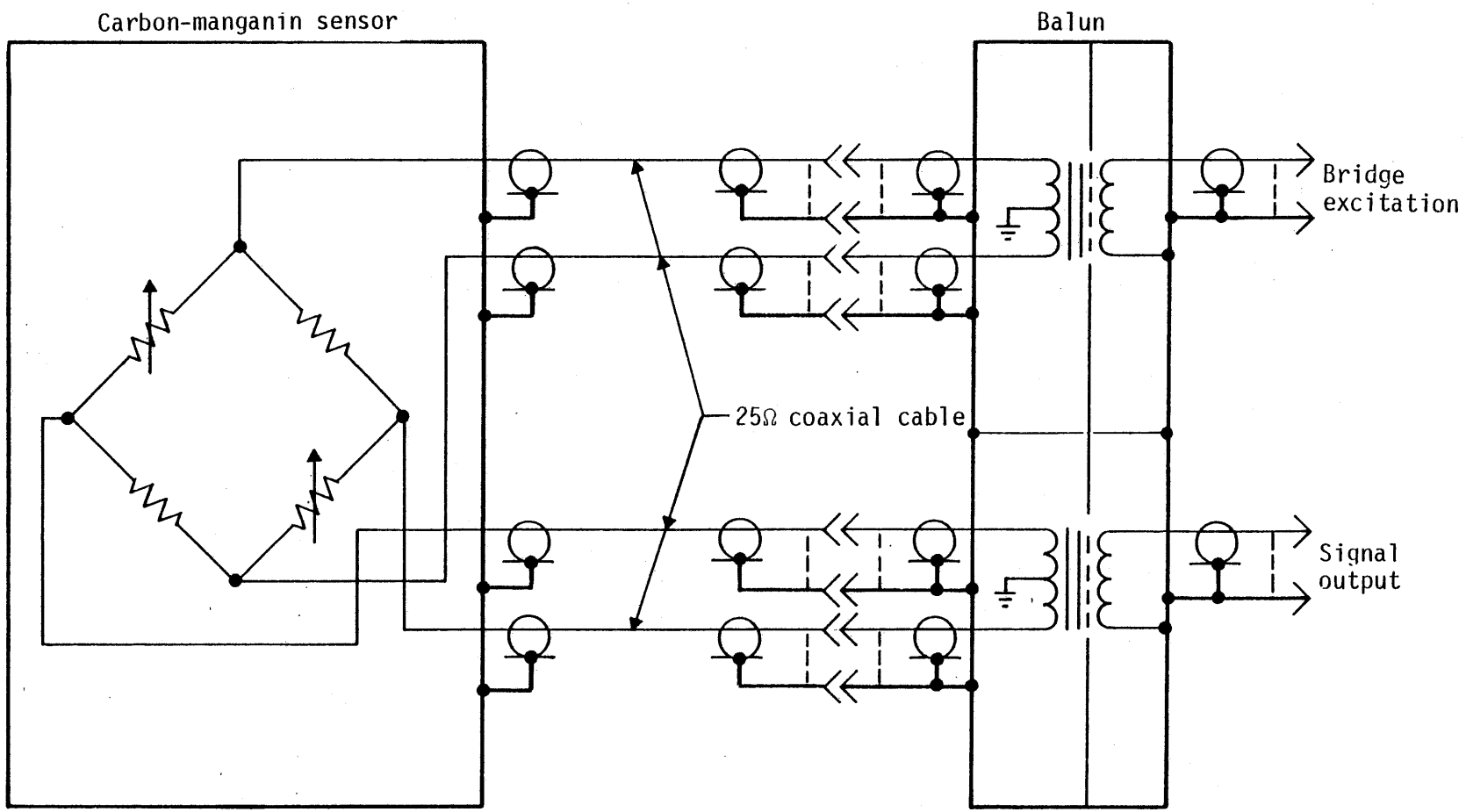

Figure 4. Carbon-manganin EMP shielding scheme.

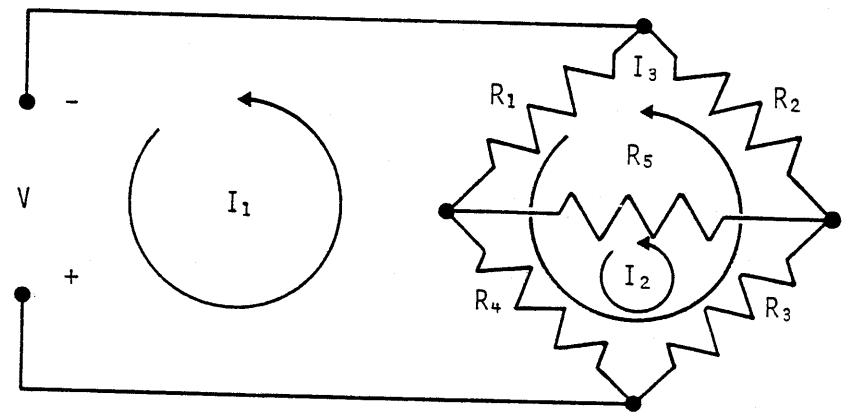

Figure 5. Terminated Wheatstone bridge.

Since the signal output is simply $I_2R_5 \equiv V'$ one first solves for I_2 using determinants:

$$I_2 = \frac{\begin{vmatrix} (R_1 + R_4) & V & -(R_1 + R_4) \\ -R_4 & 0 & (R_3 + R_4) \\ -(R_1 + R_4) & 0 & (R_1 + R_2 + R_3 + R_4) \end{vmatrix}}{\begin{vmatrix} (R_1 + R_4) & -R_4 & -(R_1 + R_4) \\ -R_4 & (R_3 + R_4 + R_5) & (R_3 + R_4) \\ -(R_1 + R_4) & (R_3 + R_4) & (R_1 + R_2 + R_3 + R_4) \end{vmatrix}}$$

$$= \frac{V \begin{vmatrix} R_4 & R_3 \\ R_1 & R_2 \end{vmatrix}}{\begin{vmatrix} (R_1 + R_4) & -R_4 & 0 \\ R_1 & R_5 & -R_2 \\ 0 & R_3 & (R_2 + R_3) \end{vmatrix}} \qquad (2)$$

Now solving for V′:

$$V' = I_2 R_5 = \frac{V \begin{vmatrix} R_4 & R_3 \\ R_1 & R_2 \end{vmatrix}}{\begin{vmatrix} (R_1 + R_4) & -R_4 & 0 \\ (R_1/R_5) & 1 & -(R_2/R_5) \\ 0 & R_3 & (R_2 + R_3) \end{vmatrix}} \tag{3}$$

or the sensitivity $\left(\frac{V'}{V}\right)$ can be written as:

$$\frac{V'}{V} = \frac{(R_4R_2 - R_3R_1)}{(R_1 + R_4)\left[R_2 + R_3 + \frac{R_2R_3}{R_5}\right] + \frac{R_4R_1}{R_5}(R_2 + R_3)} \tag{4}$$

This equation can be used to determine the sensitivity of the gage, but it should be recalled that V is the voltage at the gage and that the impedance of the signal circuit includes line resistance and transformer-insertion loss. If this is calculated for a given circuit and if it is assumed that all the initial resistances are 50Ω, that R_2 and R_4 are carbon gages, and that R_1 and R_3 are 50Ω manganin gages, the plot of the values of the sensitivity up to 20 kbars (Fig. 6) shows that the gage responds in an approximately linear manner with a sensitivity of 11 mV/V/kbar. Thus the gage can be calibrated. However, it should be noted that the values for the sensitivity will always, in a real system, be less than this because of losses in the system.

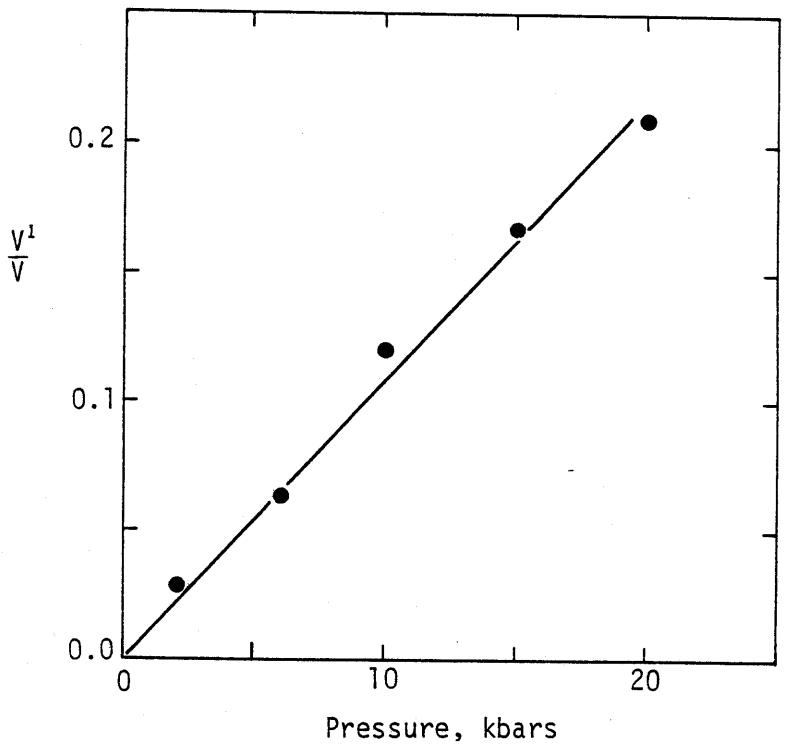

Figure 6. Theoretical output of a 50Ω carbon-manganin gage terminated at 50Ω.

III. GAS GUN TESTING

There were two sets of gas gun tests done in connection with this program. The first of these was a set of two shots done at Dynasen in Goleta, California. The second was a set of 10 shots done at the Air Force Weapons Laboratory Impact Facility operated by Ktech Corporation.

DYNASEN SHOTS

The first set of shots had the purpose of determining if possible capacitive coupling between the different elements required any modification to the gage design. In order to accomplish this, four Constantan gages were chosen and laid down in a plexiglass target in a manner duplicating the expected morphology for the carbon-manganin gage. This structure was to overlap the 12-mm by 6-mm gage elements in the manner shown in Figure 7. The gage was powered with a pulsed power supply, and the change in the resistance of the entire bridge was recorded on an oscilloscope.

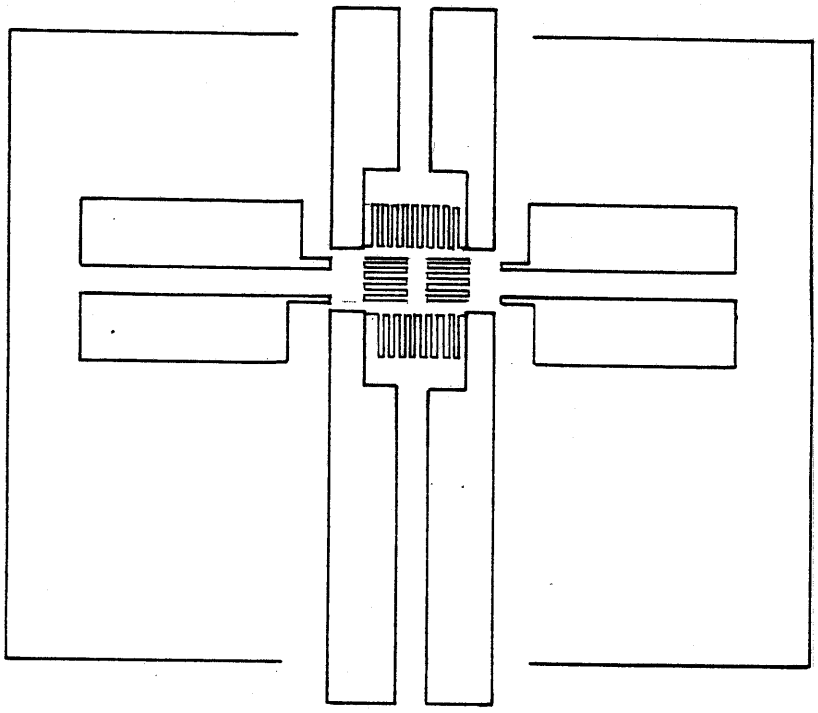

Figure 7. Actual Constantan gage overlap for Dynasen gas gun experiments.

The reason for using Constantan gages was that they have a pressure coefficient virtually equal to zero. It was thus felt that the resistance change observed in the bridge would be related primarily to the change in capacitive coupling with some possible minor strain effects caused by the possible nonplanarity of impact.

The results of the two experiments were remarkably similar in that the first one gave a resistance change of the order of 0.16 percent (Fig. 8), and the second gave a change of the order of 0.13 percent. The peak impact pressure was 6.2 kbars in both cases, and these values are more than an order of magnitude below what carbon would have changed at that pressure. Therefore, the effect was felt to be negligible, and impact gage construction at Dynasen was begun.

IMPACT FACILITY SHOTS

The next set of tests, carried out at the AFWL Impact Facility, was a series of 10 shots in the 4-in-diameter gas gun. The purpose of these tests was to excite the gage with pressure pulses to determine if the gage would survive

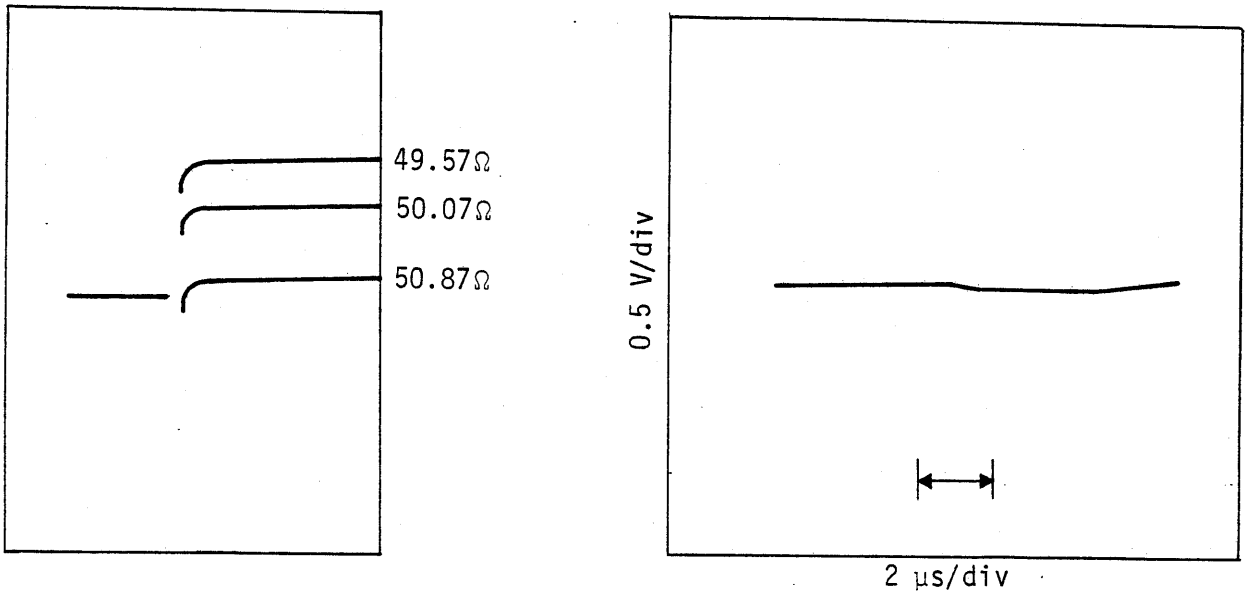

a. Calibration.

b. Gage output.

Figure 8. Results of one of the Dynasen experiments.

and give an explainable output. The original plan was to test between 1 and 10 kbars; but, since survival was not a problem, the gage was tested at the maximum (~20 kbar) this facility could provide and still have a symmetric condition for the gage mounting material.

The symmetric impact conditions were desired in order to more closely define the impact wave conditions. Given a material in a hydrodynamic condition, the stress (σ) can be expressed as $\sigma = \rho_o U_s U_p$ where ρ_o is the initial density, U_s is the shock velocity, and U_p is particle velocity. If the stress wave is generated by high-velocity one-dimensional impact, then the conservation of momentum dictates that the compressive stress wave has a partial velocity equal to one-half of the impact velocity. Thus the stress can be inferred by actively measuring the impact velocity and shock velocity and knowing the initial density.

The gages were mounted in a slow-curing epoxy (Hysol® 2038). Reference 11 describes the manner in which these were mounted in the gas gun and the procedure for their alignment. The mechanical results of 10 shots (as taken from Reference 11) are given in Table 1. It is noted that two values of stress are given. The reason for this is that σ_1 is the value calculated from the shock velocity, and σ_2 is the value obtained when using the Hugoniot equation given at the bottom of Table 1 and obtained from Reference 12. The shock velocity is determined by measuring the average time of arrival at the four planarity pins and the initial arrival at a quartz gage on the rear surface of the specimen. The measurement was felt to be somewhat inaccurate since the relative softness of this type of epoxy made it virtually impossible to make the surface flat using normal polishing techniques. On the other hand, this author feels that, although all epoxies are not identical, they are extremely similar in these responses. In other words, for the epoxy the Hugoniot equation is a good guide but not absolutely correct. Therefore, when evaluating the gage, the value used for the stress is the range of values between the values of σ_1 and σ_2.

---

11. Tarbell, W.W., *Piezoresistive Bridge Stress Gage Gas Gun Experiments*, Ktech Corporation report TR78-3, Albuquerque, August 1978.

12. Gwess, T.R., *Some Dynamic Properties of an Epoxy*, SC-DR-67-343, Sandia Laboratories, Albuquerque, June 1968, as reported in Tarbell, Ref. 11.

TABLE 1. SUMMARY OF EXPERIMENTAL PARAMETERS FOR PIEZORESISTIVE STRESS GAGE CALIBRATION

Shot no.	Impact velocity, mm/μs	Particle velocity, mm/μs	Shock velocity,[b] mm/μs	Stress		Remarks
				σ_1,[c] kbar	σ_2,[d] kbar	
1025	0.0577	0.0289	a	0.63	0.87	No tilt data.
1017	0.0551	0.0276	2.83	0.86	0.83	
1018	0.1142	0.0571	a	---	1.74	No tilt data.
1022	0.1561	0.0781	2.49	2.15	2.41	
1020	0.3399	0.1699	2.67	5.01	5.49	
1023	0.4299	0.2150	2.57	6.10	7.11	
1016	0.5310	0.2655	2.93	8.59	9.00	
1019	0.5581	0.2791	2.82	8.69	9.51	
1021	0.5626	0.2813	2.85	8.85	9.60	3.175-mm thick PMMA flyer.
1024	1.0715	0.5358	3.24	19.17	20.46	6.35-mm thick PMMA flyer.

[a] Shock velocity not measured.

[b] Transit time from impact to quartz gage breakaway.

[c] $\sigma_1 = \rho U_s U_p$; $\rho = 1.104$ g/cm^3; U_s = shock velocity; U_p = particle velocity.

[d] $\sigma_2 = \frac{1.104}{1.200} (32.30\ U_p + 17.45\ U_p^2)$ (Ref. 12)

PMMA = polymethylmethacrylate

The first five tests of this series should be viewed as setup experiments because a number of electrical difficulties were encountered and overcome during this series. For example, the Tektronix 180A time-mark generator used as a 10-MHz power source was apparently loading down. It was replaced with another unit not exhibiting this fault. Also, the connections between the elements were at first made with buss wire (normally 20 gage). It was found that, for this wire at 10-MHz, 1 inch of wire equaled 1 ohm of resistance. Thus, this wire added extraneous resistance and bridge upset that was not expected. This problem was corrected by replacing the connections with a heavy braid (RG58 shield).

Thus the data from the first five shots (1016 through 1020) are not considered here. Only those from the last five shots (1021 through 1025) are used. These data are given in Figures 9 through 13. The bridge was artificially upset with a resistor that effectively lowered the resistance of the carbon legs so that there were no zero crossings. It was thus insured that the signal direction would be an increase in voltage.

Figure 12 is an excellent example of one of the primary advantages of using alternating current (ac) as opposed to direct current (dc) bridges.

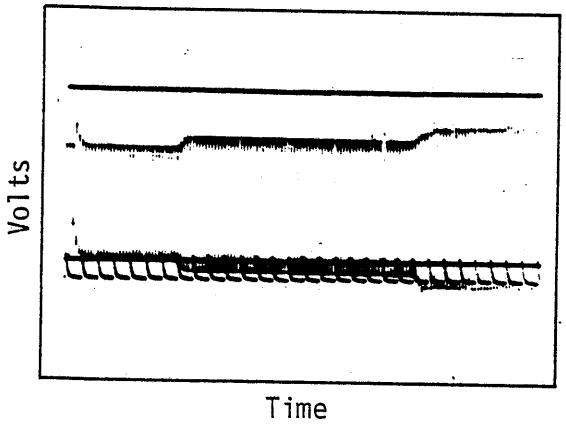

Note: Time marks at 0.5-μs intervals.

Figure 9. Shot no. 1025; calibration level, 100 mV.

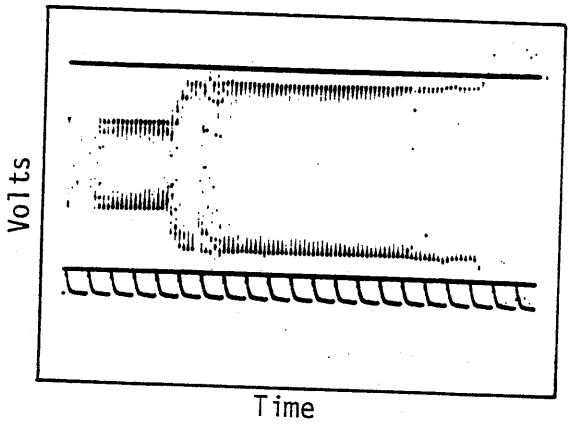

Note: Time marks at 0.5-μs intervals.

Figure 10. Shot no. 1022; calibration level, 150 mV.

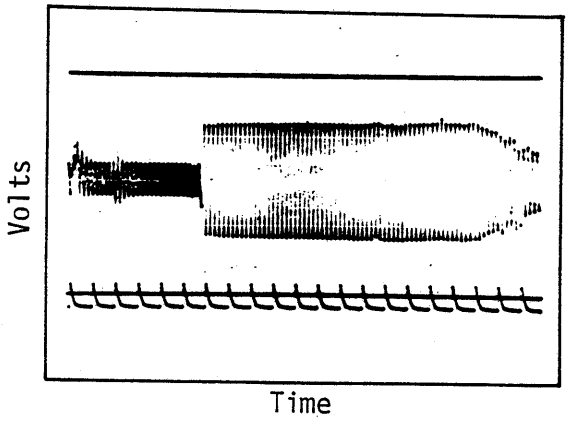

Note: Time marks at 0.5-μs intervals.

Figure 11. Shot no. 1023; calibration level, 500 mV.

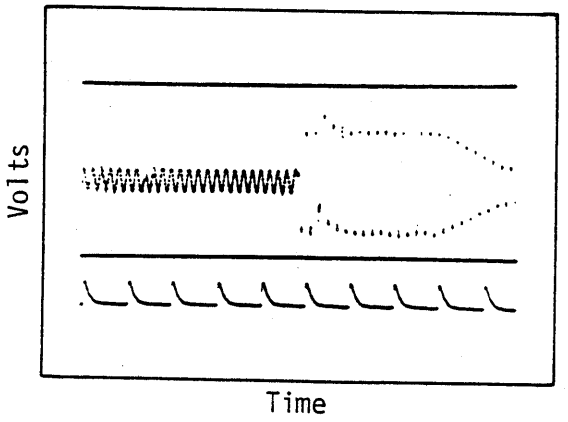

Note: Time marks at 0.5-μs intervals.

Figure 12. Shot no. 1021; calibration level, 400 mV.

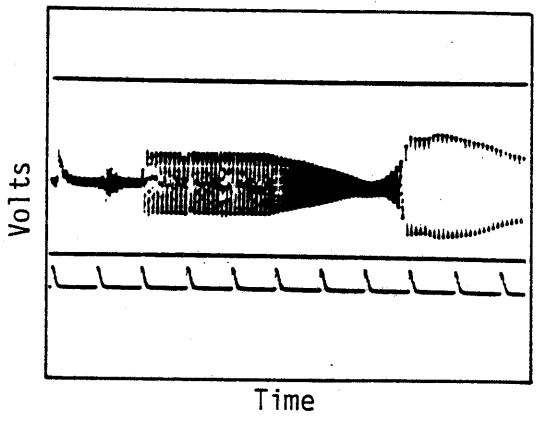

Note: Time marks at 1-μs intervals.

Figure 13. Shot no. 1024; calibration level, 1500 mV.

On this test, the fiducial pulse used to normalize times on the different traces arrived at a later time than expected. In fact it arrived 2 μs after shock arrival at the gage. It is clearly identifiable as something caused by a source other than gage response since there is an offset in the gage output rather than a symmetric increase or decrease in the 10-MHz oscillation.

The data are summarized in Table 2 and Figure 14. The most surprising feature in the plot in Figure 14 is the linearity of the data.

TABLE 2. CARBON-MANGANIN GAGE PERFORMANCE

Shot no.	Input, V	Output, mV	Normalized	Rise time, μs	Stress, kbars
1025	3.714	11.2	3.02	0.3	0.63 to 0.87
1022	3.860	57.6	14.92	0.4	2.15 to 2.41
1023	3.966	189.0	47.76	0.1	6.10 to 7.11
1021	3.162	169.0	5357.00	0.1	8.55 to 9.51
1024	3.451	440.0	127.50	0.1	19.17 to 20.46

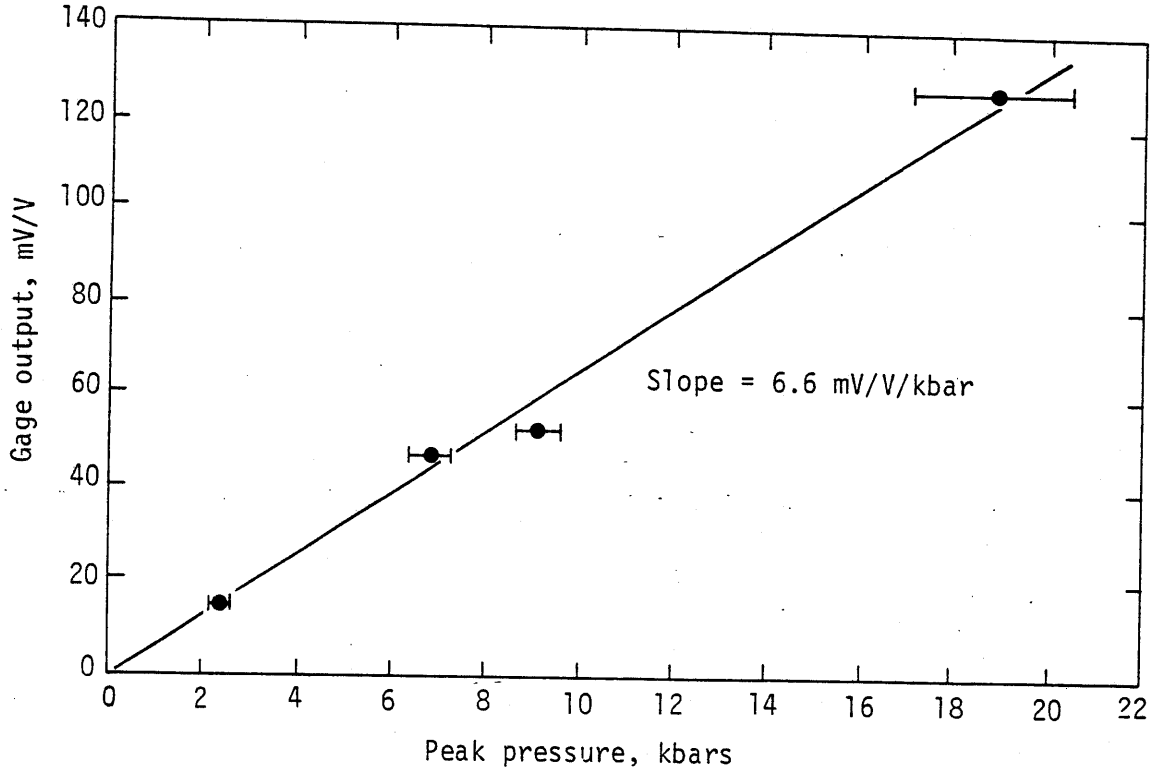

Figure 14. Carbon-manganin gage output versus peak pressure.

IV. HIGH-EXPLOSIVE TESTING

There was a series of three high-explosive tests performed on the carbon-manganin gage. The purpose of these tests was to determine if the gage could survive pulses of longer duration than those imparted in the gas gun; the tests were also intended to lead to the design and construction of a fieldable gage suitable for use on an underground test. The high-explosive tests were dubbed the Manganin and Carbon Explosives (MACE) tests. The gage construction, the test layout, and the test results are described below.

GAGE CONSTRUCTION

The individual carbon and manganin gage elements were constructed at Dynasen. They were made under specifications supplied by NMERI. Each gage was nominally 50Ω. The leads were aluminum and were 40 cm long. The aluminum was chosen because of its low sensitivity to neutrons and its better mechanical impedance match to the epoxy in which it was to be encapsulated (Fig. 15). The 40-cm length was chosen because it was physically the longest gage lead that Dynasen could make with their equipment. The leads for the individual gages had solder tabs near the element in order that they might be connected close to the bridge. This was done for electrical symmetry and to lower the effective lead resistance.

Using these elements, EG&G constructed the actual gage. Figure 16 is a drawing of the gage. The solid aluminum jacket for the 25Ω cable was constructed (by special order) by Uniform Tube. The aluminum foil covering the exterior of the gage was 0.05 mm thick. The legs were made of cast epoxy. (The reason for using epoxy is again evident in Fig. 15.) Each leg containing the leads for the individual elements was nominally 25 mm thick by 51 mm wide. These dimensions were chosen in order that the characteristic impedance of each of the lead conductors with respect to the outer shield would be 50Ω. Thus, when combined with the parallel lead going to the same corner of the bridge, the characteristic impedance of 25Ω, or that of the aluminum coaxial cable (coax), was achieved. After assembly, the gage was painted in order to prevent any reaction between it and the grout in which it was to be placed. The overall dimensions of the gage are 25 cm in diameter by 40 cm in length.

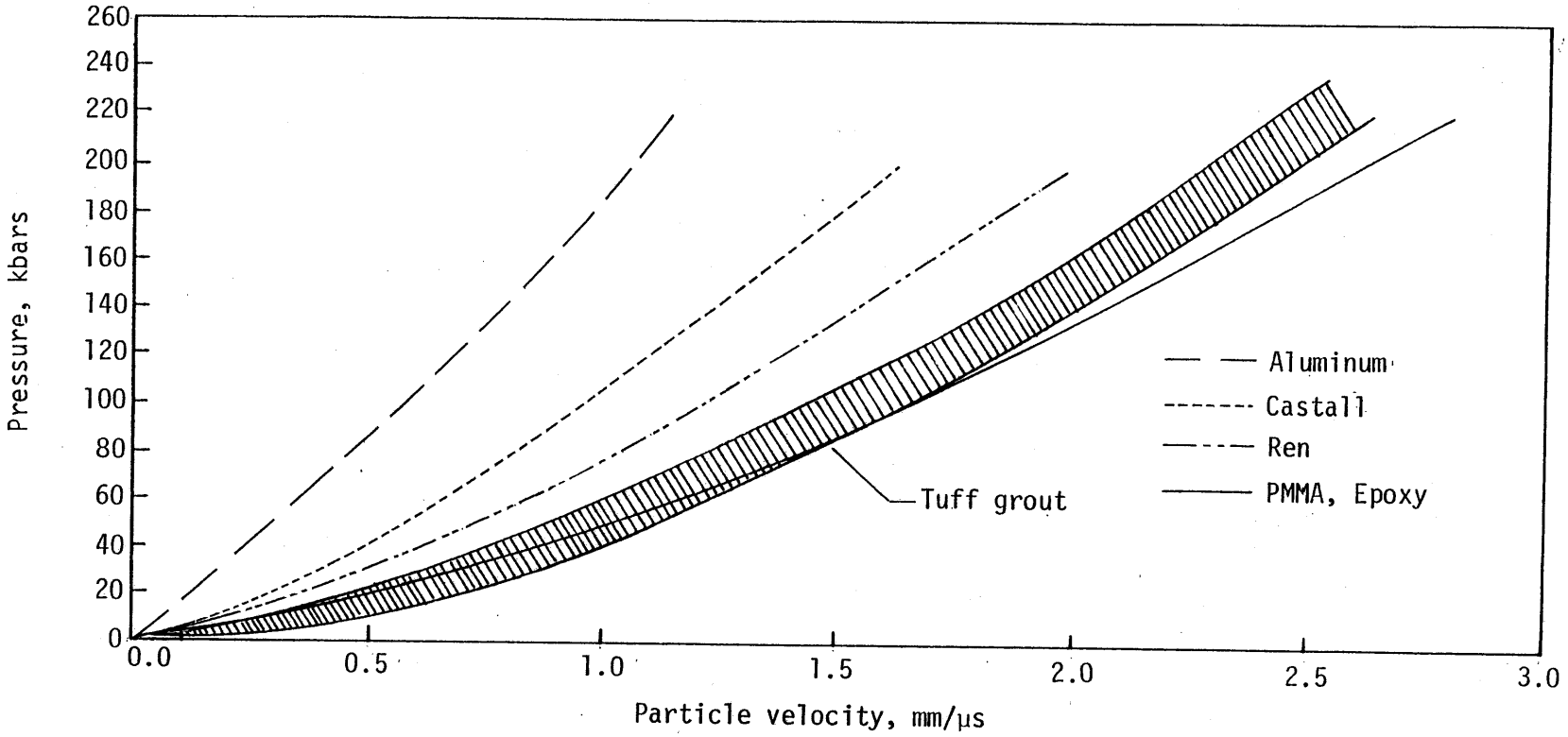

Figure 15. Hugoniot's function, showing grout, epoxy, and aluminum.

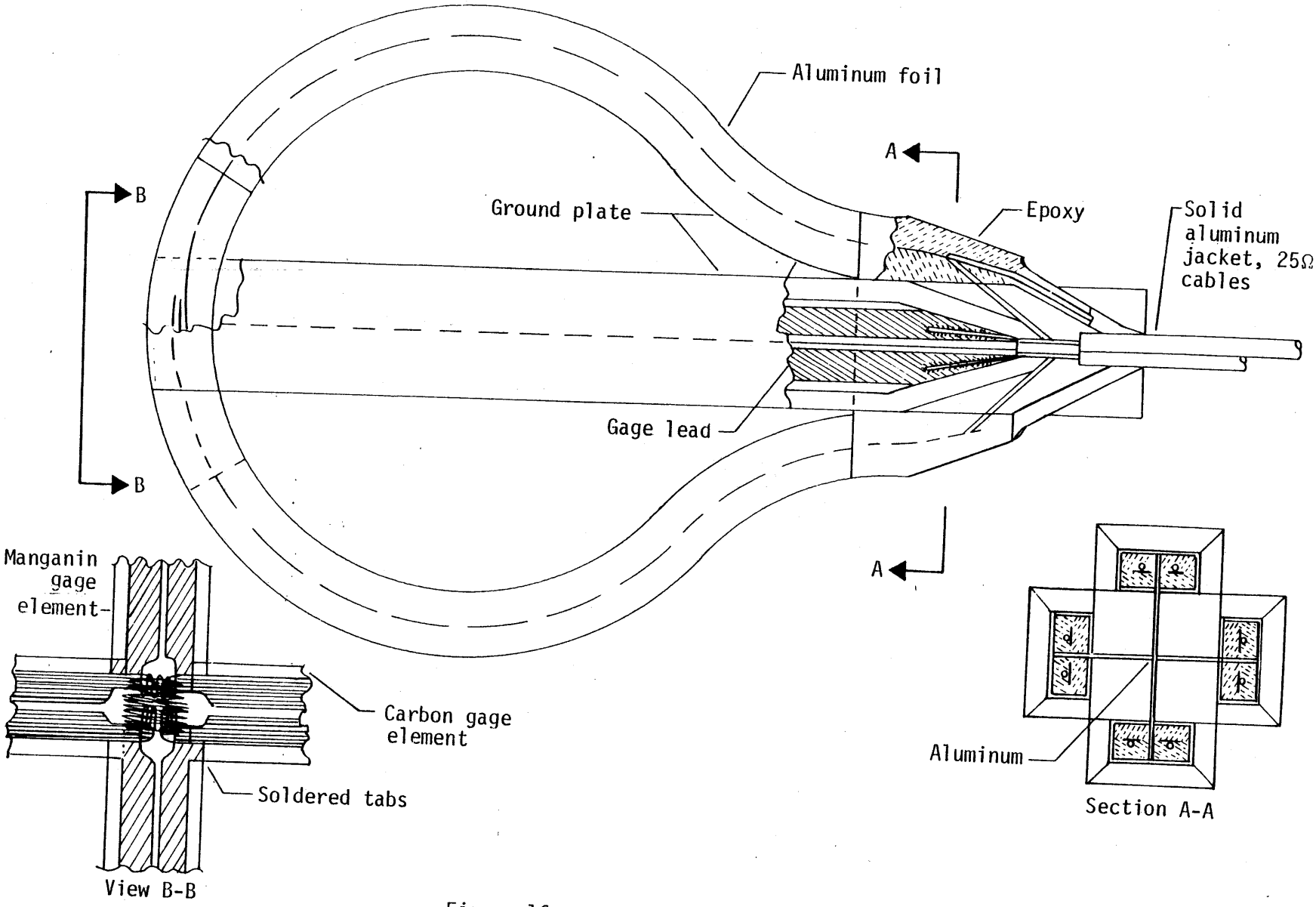

Figure 16. Carbon-manganin gage.

There was one particularly nagging problem associated with the gage. This was the strength of the bond between the cable and the foil lead. Numerous times this connection broke, probably because of cable bending. This problem was finally corrected by soldering a copper plate to the foil leads and attaching the coax to that connector.

TEST LAYOUT

The test bed was constructed in the manner indicated by Figure 17. The gage was cast in grout. Piezoelectric pins were used to determine planarity of impact and shock velocity. The explosive charge consisted of 23 blocks of C-4, a military plastic explosive. The total mass of explosive in each shot was 13.5 kg. The cavity was 0.3 x 0.3 x 0.2 m. The overburden density was nominally 1760 kg/m^3. These parameters were chosen because the HEST Design Lockup Model predicted a 10-kbar peak equilibrium cavity pressure and a 2-ms fall to half of peak pressure. These predictions were made with the caveat that the code had never been used for predicting pressures this high; the cavity expansion model was probably incorrect because of material model deficiencies at the higher pressures. Thus these pressure values are only approximate.

A schematic of the instrumentation layout is given in Figure 18. All of the pins functioned correctly on the first MACE test but not on the other two. On MACE 2 planarity could not be determined, and on MACE 3 the primary gage channel failed to trigger. For this reason, only the results of MACE 1 and 2 are given.

TEST RESULTS

The gage outputs for MACE 1 and 2 are given in Figures 19 and 20. The MACE 1 data indicate that the peak pressures achieved were of the order of 15 to 16 kbars; after about 2 μs, the pressures quickly fell to the order of 1 kbar. These data do not appear to be valid pressure data, probably because there was some strain induced on the elements. The planarity of the shock was poor in this shot (~3.5 μs) across the gage surface. The gage elements each have a strain gage factor of approximately 2. Signals caused by strain may thus be misread as uniaxial flow. MACE 2, on the other hand, gave data that were somewhat like that expected. The pressure rose in approximately

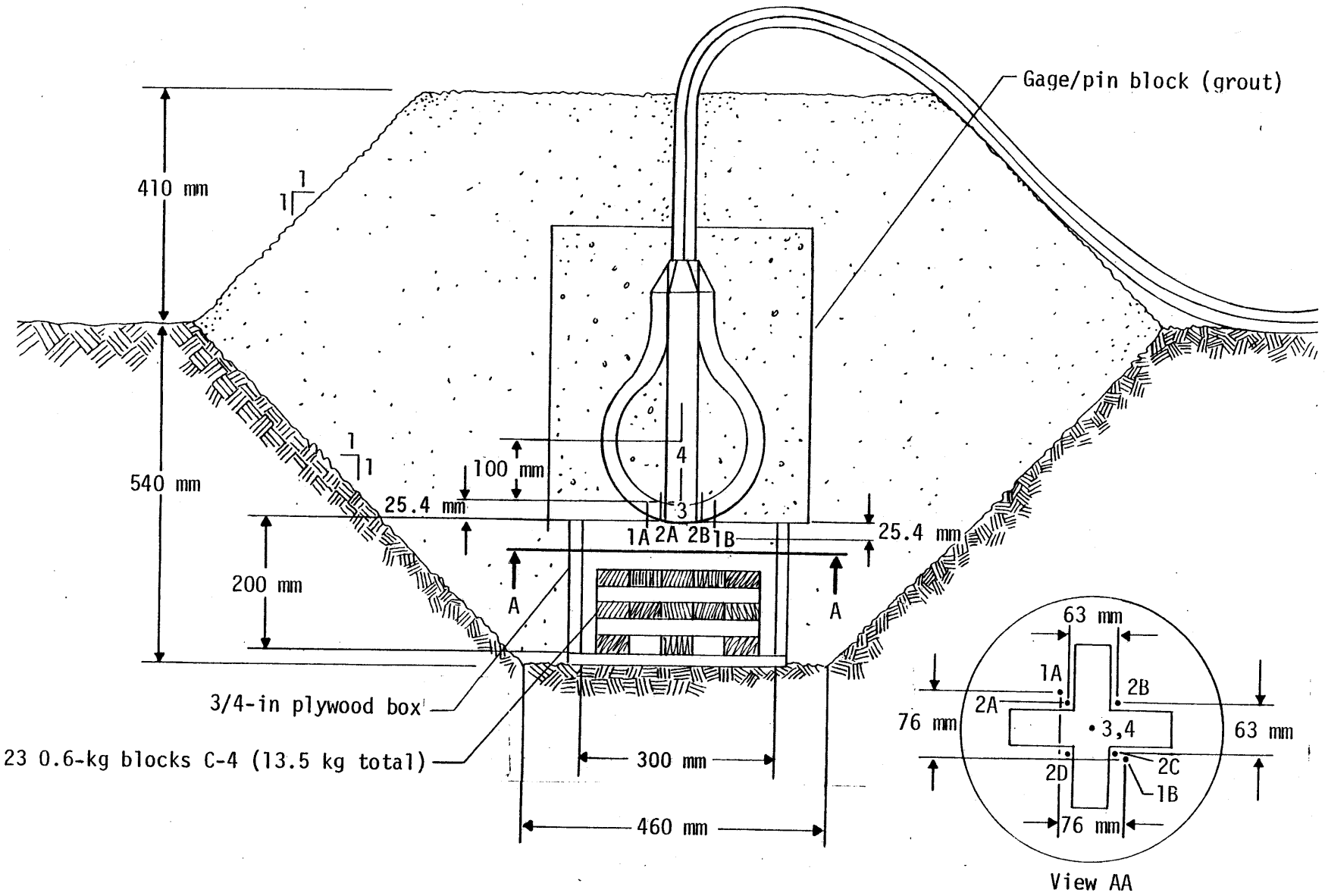

Figure 17. Manganin and carbon explosive test 1, test bed layout.

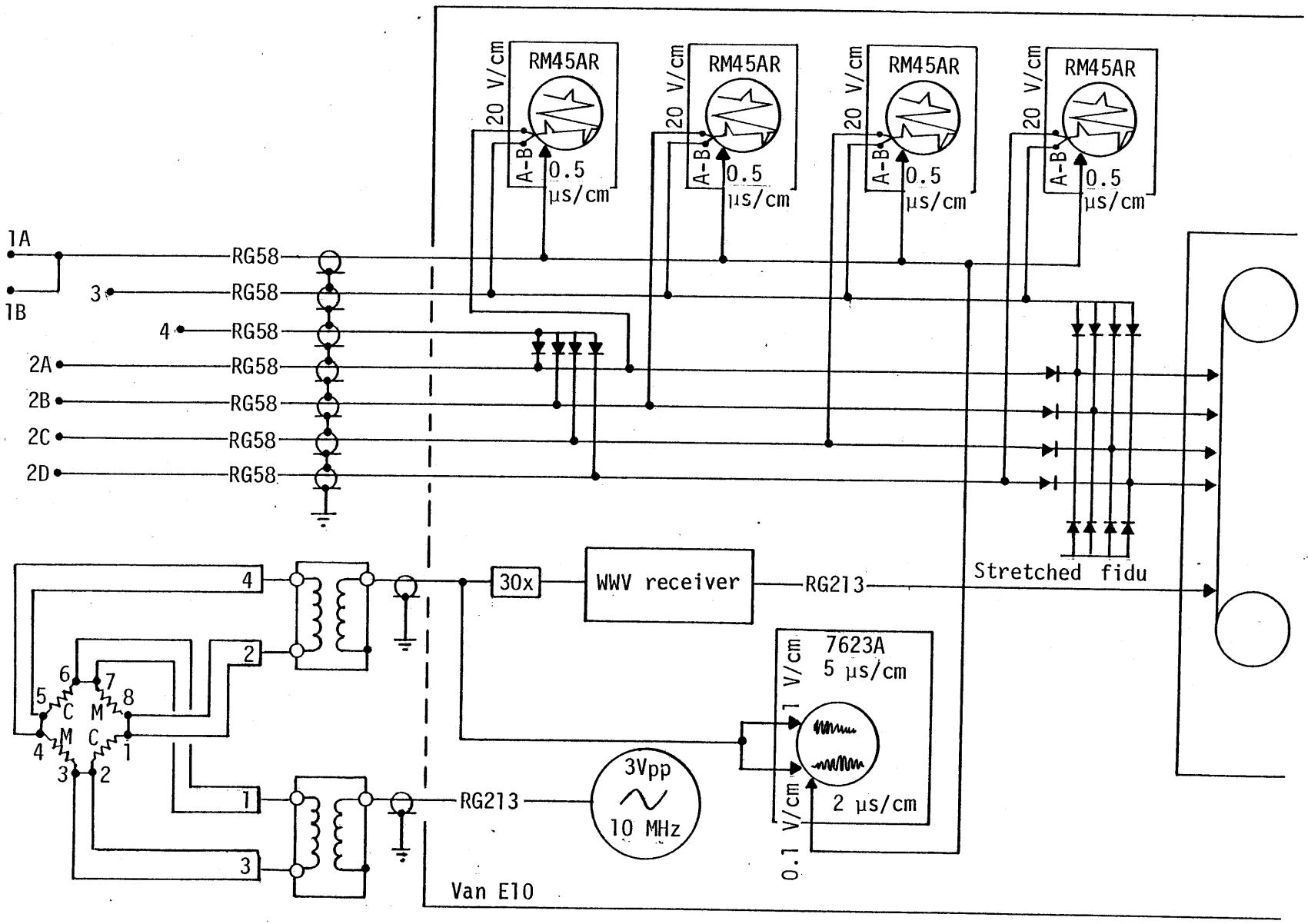

Figure 18. Carbon gage and TOA pin instrumentation, MACE 1.

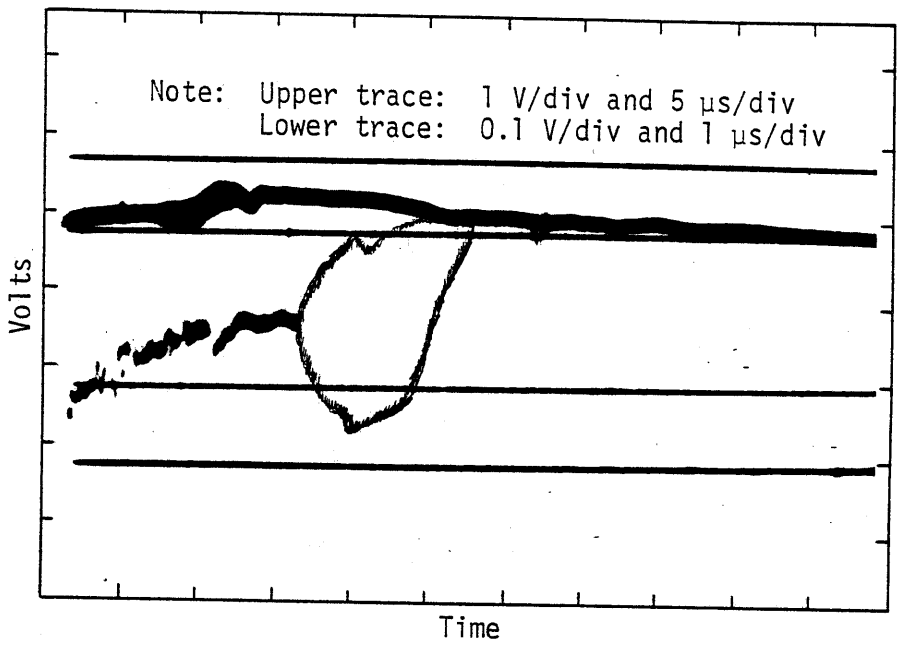

Figure 19. MACE 1 carbon-manganin gage output.

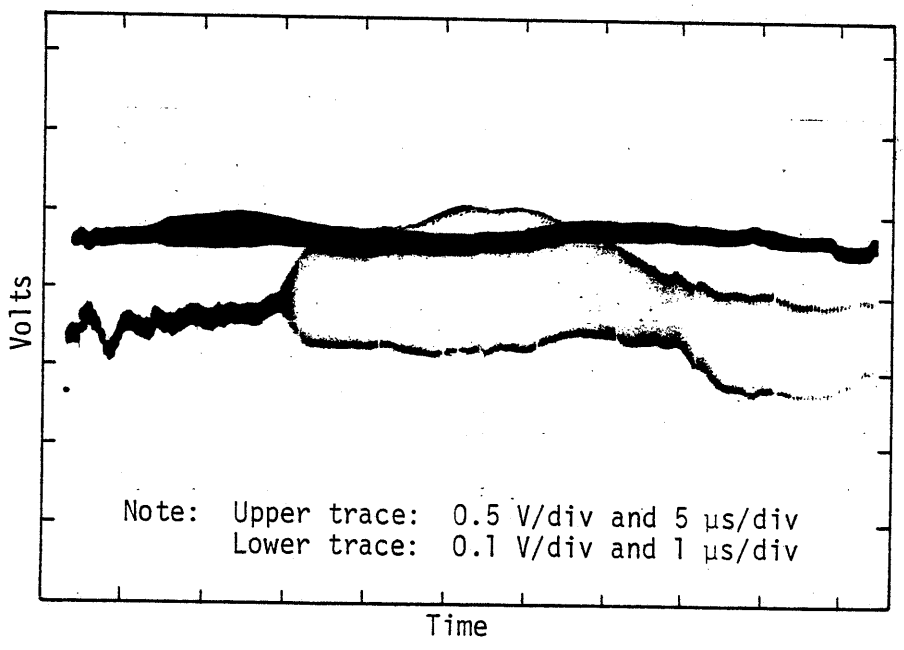

Figure 20. MACE 2, carbon-manganin gage output.

0.5 μs to 9 kbars and then began to decay with one minor oscillation in the envelope at about 5 μs after shock arrival.

The low-frequency noise observed on top of the data is somewhat discomforting but not disabling. It is presumed that either the aluminum foil shield was not effective enough or that the noise was generated inside the van. The latter appears to be the more likely cause.

One of the failure modes observed after the test was the delamination of the arms of the sensor on the plane of the individual gage elements (Fig. 21). It is felt that this failure occurred not only because of the presence of the inclusion but also because of the construction technique. Two distinct epoxy pours were used. The first mold was allowed to harden; it was then machined, and the gages were placed on it. Then a second pour was made. This process probably resulted in a poor bond between the layers.

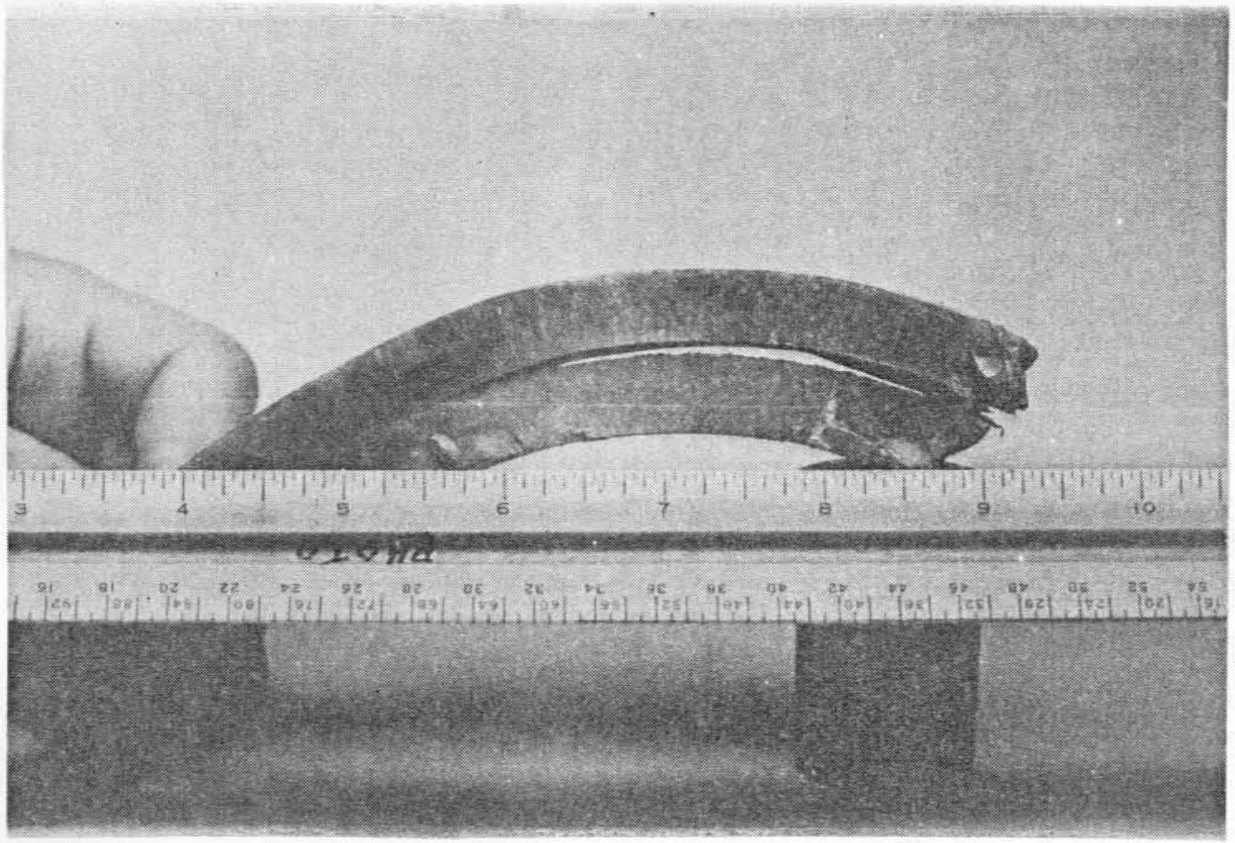

Figure 21. Photograph of delamination of gage arm after the test.

V. TRANSIENT RADIATION EFFECTS

In order to determine whether the gage was susceptible to the electrical noise generated on an underground test, the gage was subject to $\dot{\gamma}$ (time rate of change of γ) testing at the Transient Radiation Effects Facility (TREF), an organization of AFWL. (See Appendix A for facility description from Ref. 13.)

The gage was tested at $\dot{\gamma}$ levels between 1×10^{11} and 3×10^{11} rad/s. In order to determine if these levels were acceptable, the predictions for HYBLA GOLD were looked at (Ref. 1). A typical gage was postulated to be 30 m down the largest tunnel and buried 7 cm in the grout.

Figure 22 gives the history of the $\dot{\gamma}$ at the wall of the tunnel. This figure shows a peak of 3.5×10^{10} rad/s. Figure 23 gives the reduction factor in the grout. If the depth of burial is 7 cm, the reduction factor is 5×10^{-3}, and the gage would receive radiation on the order of 1.8×10^{8} rad/s. Thus it was felt that an environment three orders of magnitude greater than this was adequate to test the gage.

The worst case is given in Figure 24. Here it is seen that there is a short pulse about equivalent in shape to the $\dot{\gamma}$ pulse (20 ns wide). There is only a slight distortion for the next 200 ns, and there is even less for the next 1 μs. The height of the first 20-ns pulse is significant in that it corresponds to a 3-kbar pressure; but its effect on a pressure reading is neglible because of the short duration. A worse effect may come from the distortion apparent for the next 200 ns, but this distortion corresponds to less than 0.5 kbar and is thus neglible. The smallness of the distortion is somewhat amazing when it is realized that 3×10^{11} rad/s corresponds to currents of 6000 A/m^2. Since the effective cross section of the gage is approximately 360 cm^2, this level corresponds to over 200 A passing through the gage and its shields.

It was thus felt that the gage was adequately protected for the expected environment for an underground test.

---

13. *TREF Simulation Facilities*, DNA-2432H, Defense Nuclear Agency, Washington, D.C., October 1973.

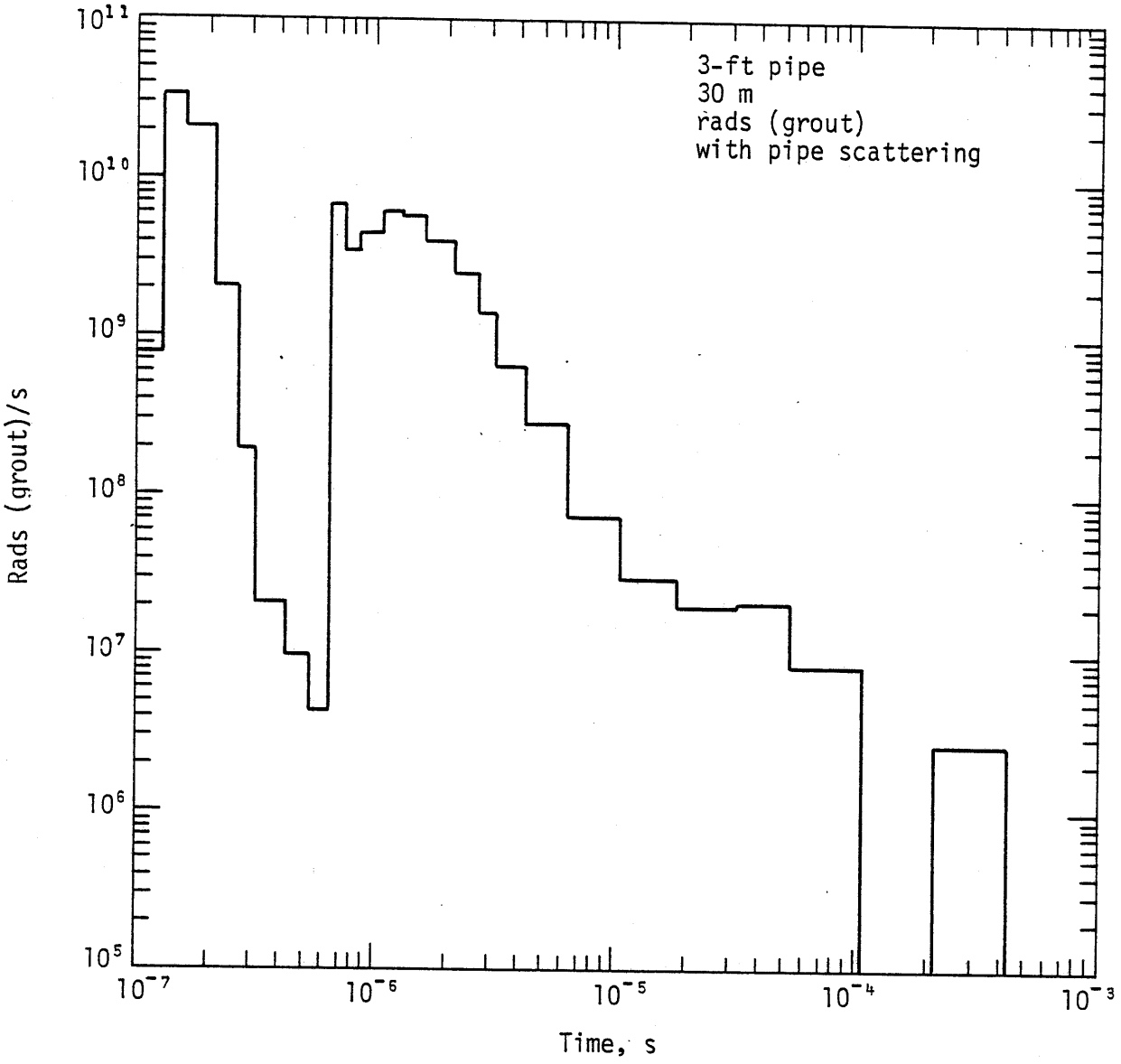

Figure 22. Time-dependent rads (grout), 30 m with pipe scattering.

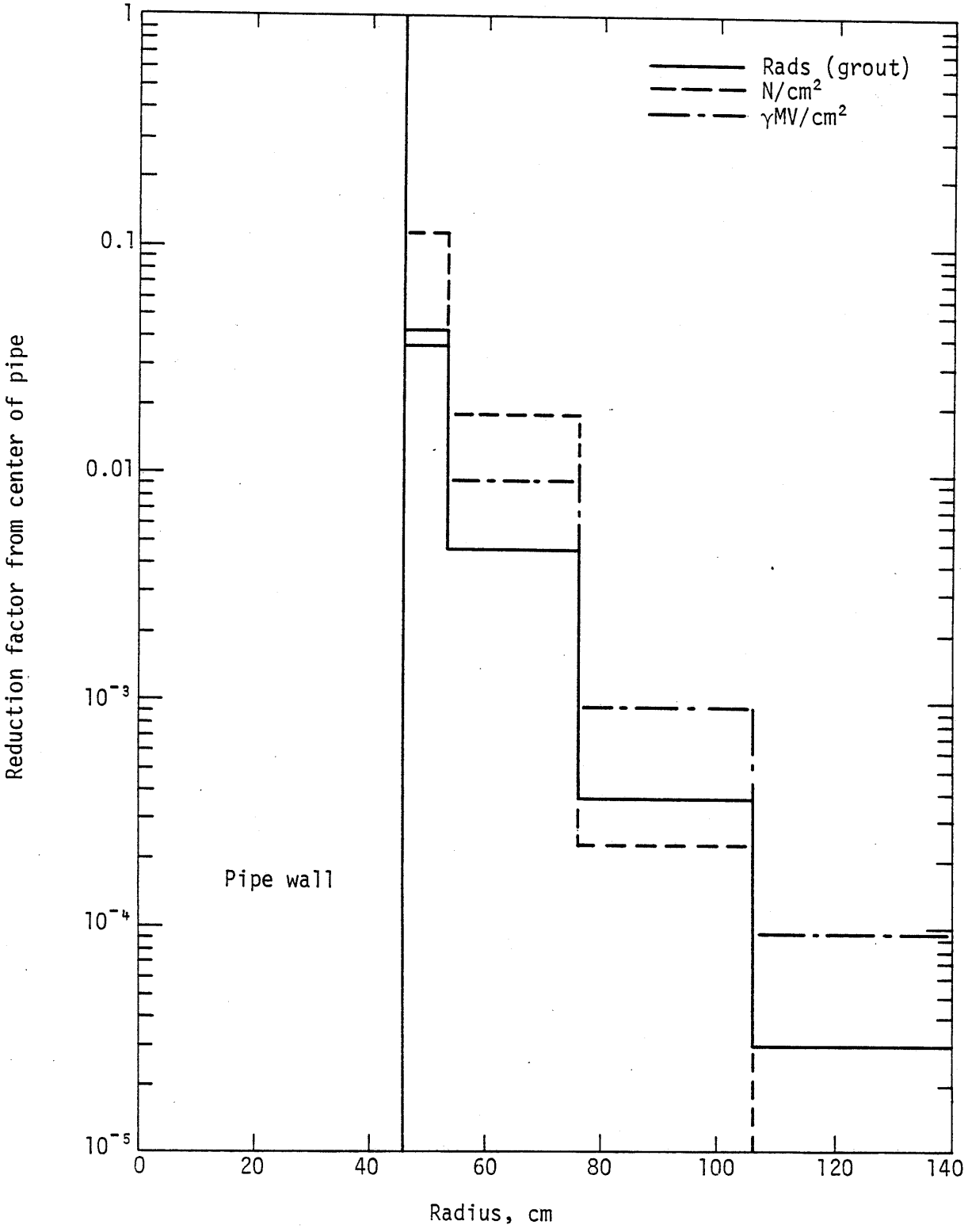

Figure 23. Reduction of dose versus depth into 3-ft pipe wall.

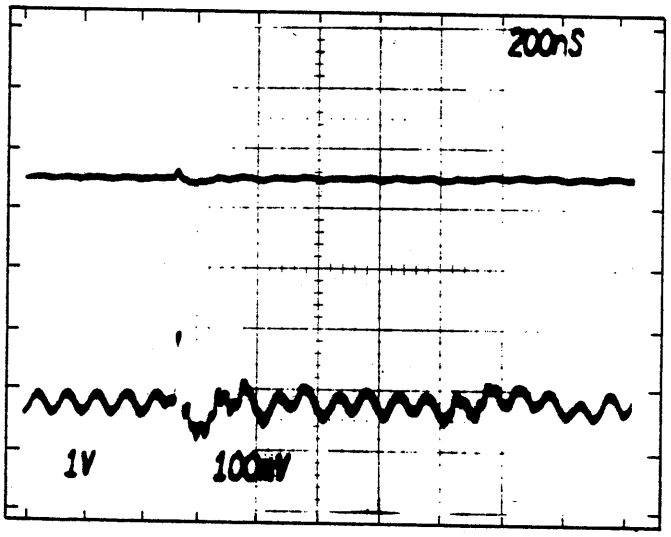

Figure 24. Worst-case carbon-manganin gage output when tested at TREF.

VI. NEUTRON EXPOSURE

The last set of tests on the carbon manganin gage was done to determine if there was any significant sensitivity of the gage to neutron exposure. The neutron bombardment produced in an underground test can be extremely harsh, especially to anything containing hydrogen. This is because the neutron will displace the hydrogen nucleus and cause a larger proton current to be generated. This problem has been recognized for a long time, yet hydrocarbons are still used in gage mountings because of the unavailability of an acceptable substitute.

The tests were conducted at the Sandia Pulsed Reactor (SPR) located at Kirtland Air Force Base. A description of the SPR facility is given in Appendix B, and a more complete description can be found in Reference 14.

There were three shots performed. The average flux in these shots was 6.9×10^{13} neutrons/cm^2. The pulse width was 50 μs. Thus the average dose rate was 1.4×10^{18} neutrons/cm^2/s. In order to determine if this was adequate, Reference 1 was again consulted. At 30 m down the 3-ft pipe on HYBLA GOLD, the predicted peak dose rate was 5×10^{18} neutrons/cm^2/s as shown in Figure 25. If the reader will simply return to Figure 23 and recall that the gage is buried 7 cm deep in the grout, then it will be clear that the reactions would be reduced by a factor of 2×10^{-2} to the net peak reactor dose rate of 10^{17} neutrons/cm^2/s. Thus a dose rate an order of magnitude greater than this should be sufficient.

Figure 26 shows typical output traces taken from the second shot. They are both from the same gage set at different sensitivities and sweep speeds. As one can see, there is no observable effect from the neutrons with the exception of a slight drift of the entire envelope of the 10-MHz signal. This drift would seem to imply that the electronics outside the test area are being affected.

---

14. Estes, B.F., and Snyder, V.A., *Sandia Pulsed Reactor Facility*, SAND79-0391, Sandia Laboratories, Albuquerque, 1979.

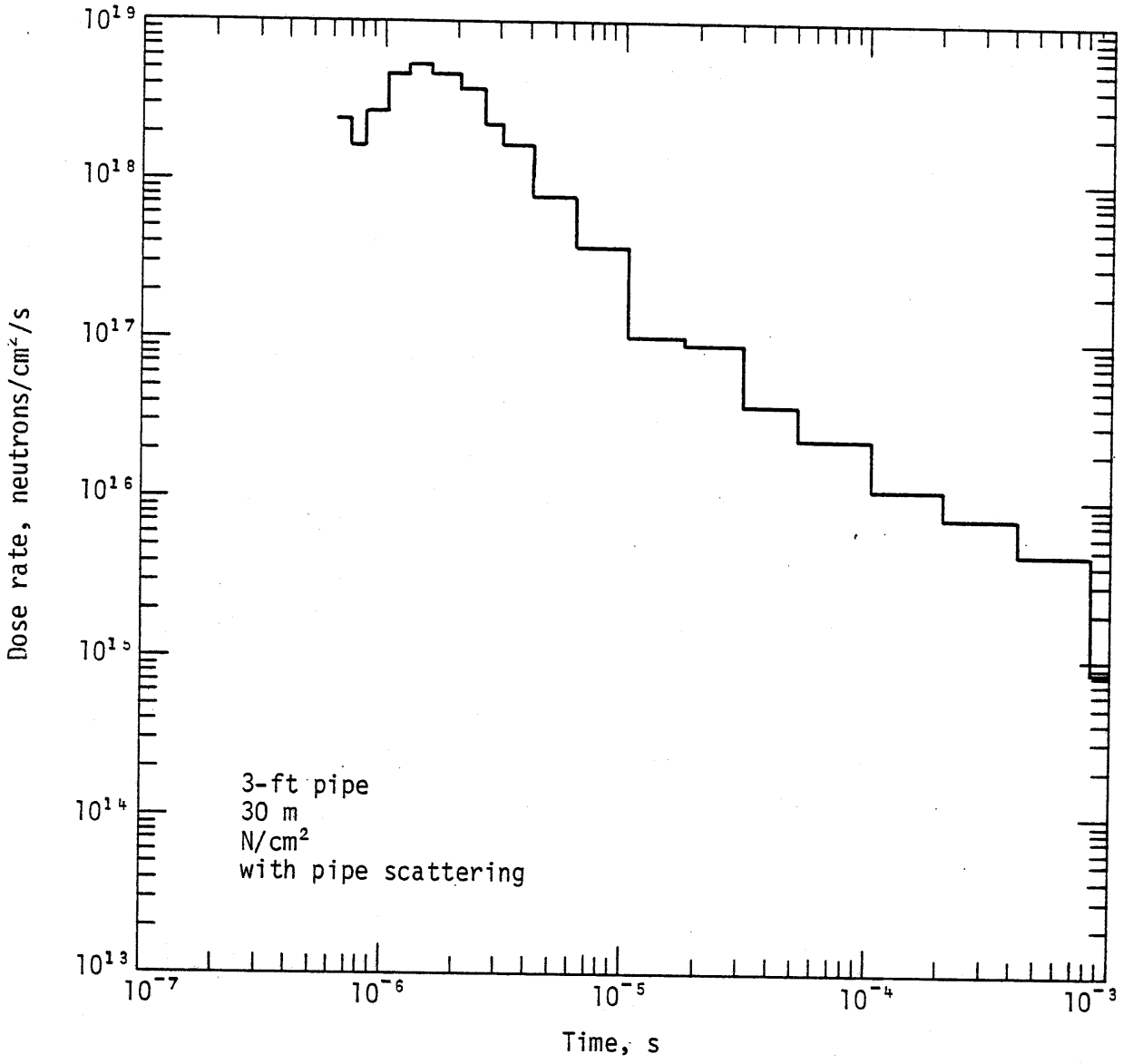

Figure 25. Time-dependent dose in the 3-ft pipe at 30 m with pipe scattering.

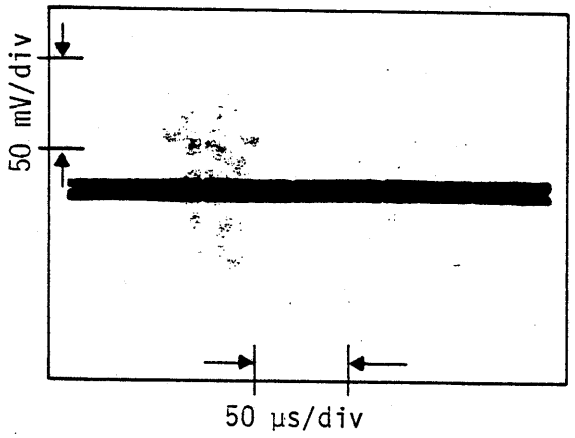

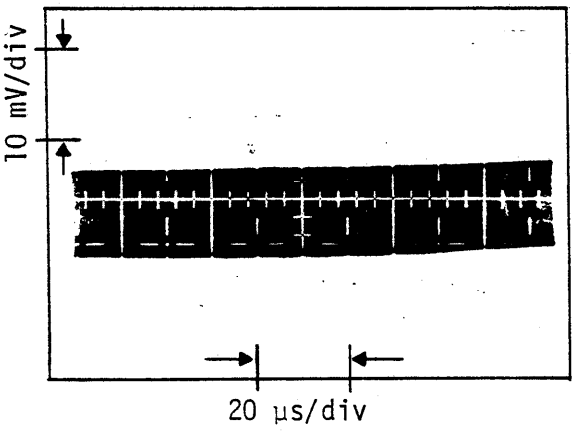

Figure 26. Output of carbon-managin gage during neutron irradiation test 2.

VII. CONCLUSIONS AND RECOMMENDATIONS

The carbon-manganin gage appears to be suitable for use in the defined environment on an underground test. The defined environment means a peak pressure of 10 kbars or less, $\dot{\gamma} < 3 \times 10^{11}$ rad/s, and neutron does rates of less than 10^{18} neutrons/cm^2/s. The survival time at 10 kbars was not really determined because of the previously mentioned failure of the demodulator. It is known that the gage did survive for greater than 100 μs under load. It is thus recommended that the gage be further tested if time and funds allow and that an adequate demodulator be developed.

Otherwise the gage appears to function well, to be linear in output to 20 kbars, and to have a low sensitivity to radiation.

A second, somewhat extraneous, point is that the advantages of using ac excitation were also noted. When working with frequencies as high as 10-MHz, the uninitiated will soon feel like a pair of brown shoes in a world of tuxedos, but the advantage in noise suppression makes the effort well worthwhile. Additionally, most of the work done in blast and shock requires much less in terms of frequency response than that desired on an underground test. In normal high-explosive tests, a 20-kHz frequency response is more than satisfactory. Thus a carrier of a few hundred kilohertz would be more than adequate. An additional advantage of ac is that one can multiplex signals in balanced transformers and record on tape. It is thus recommended that ac excitation be considered for use on all bridge gages used in normal blast and shock testing.

REFERENCES

1. *HYBLA GOLD Radiation Environment Progress Report*, SAI-77-700-LJ, Science Applications, Inc., La Jolla, California, June 1977.

2. Charest, J.A., *Development of a Carbon Shock-Pressure Gage*, DNA-3101F, Defense Nuclear Agency, Washington, D.C., 31 July 1973.

3. Naumann, W., *Carbon Stress Gage Development*, Final Report DNA-3027F, Defense Nuclear Agency, Washington, D.C., April 1973.

4. Ginsberg, M.J., DeCarli, P.S., and Dempster, J., *Minute Gun Series* (U), *Diamond Sculls Event* (U), *Carbon Gage Measurements* (U), a confidential report POR 6724, Defense Nuclear Agency, Washington, D.C., 10 October 1973.

5. *Carbon Shock Pressure Gages*, Data Sheet No. 2, a brochure from Dynasen, Inc., Goleta, California.

6. *Specification, Carbon Stress Gage*, Effects Technology, Inc., Santa Barbara, California, 14 July 1972.

7. Steele, E.J., and Naumann, W.J., *Minute Gun Series* (U), *Diamond Sculls Event* (U), *Carbon Gage Evaluation in Diamond Sculls* (U), an S-RD report, POR 6730, Defense Nuclear Agency, Washington, D.C., 10 October 1973.

8. Ginsberg, M.J., *Calibration and Characterization of Ytterbium Stress Transducers*, DNA-2742F, Defense Nuclear Agency, Washington, D.C., October 1971.

9. Smith, C.W., et al., *Constitutive Relations from In Situ Lagrangian Measurements of Stress and Particle Velocity*, DNA-28831, Defense Nuclear Agency, Washington, D.C., January 1972.

10. Baum, N., *Topological Concepts as Applied to Electrical Signal Isolation and Mechanical Cable Survivability*, BAS Instrumentation Notes, Note 1, Feb 1980, Air Force Weapons Laboratory, Kirtland AFB NM

11. Tarbell, W.W., *Piezoresistive Bridge Stress Gage Gas Gun Experiments*, Ktech Corporation report TR78-3, Albuquerque, August 1978.

12. Gwess, T.R., *Some Dynamic Properties of an Epoxy*, SC-DR-67-343, Sandia Laboratories, Albuquerque, June 1968, as reported in Tarbell, Ref. 11.

13. TREF *Simulation Facilities*, DNA-2432H, Defense Nuclear Agency, Washington, D.C., October 1973.

14. Estes, B.F., and Snyder, V.A., *Sandia Pulsed Reactor Facility*, SAND079-0391 Sandia Laboratories, Albuquerque, 1979.

APPENDIX A

TREF FACILITY DESCRIPTION
(from Ref. 13)

3.8 AFWL TRANSIENT RADIATION EFFECTS FACILITY (TREF)

Air Force Weapons Laboratory
Kirtland Air Force Base
Albuquerque, New Mexico

CHARACTERISTICS

The Air Force Weapons Laboratory (AFWL) Transient Radiation Effects Facility (TREF) is a gamma-radiation simulation test laboratory specifically designed for conducting transient-radiation-effects experiments. The radiation environment is produced by two super flash X-ray machines: the FX-100 (Figure 3.8-1) and the Model 1590 (Figure 3.8-2).

The beam center lines of the two machines intersect perpendicularly at a point 75 cm in front of the respective X-ray tubes. The intersection point is the prime test position and is located within a specially designed, doubly isolated RF enclosure within the experimental test cell. The enclosure is an integral part of the instrumentation room which is the prime data acquisition terminal.

The two machines, although designed and built by different manufacturers are basically similar in that stored, electrical energy is switched into a cold-cathode electron tube producing an intense beam of electrons which is converted into bremsstrahlung by means of the thick-target tantalum anode.

The two machines may be fired independently, simultaneously, or sequentially to give higher dose rates or total dose to large test samples.

The laboratory contains approximately 20,000 ft^2 of useful space (Figure 3.8-3). It houses the flash X-ray machines, machine maintenance areas, experimental test cell, diagnostic and control rooms, calibration rooms, user support areas, laboratories for radiation dosimetry measurements, and an instrumentation, fabrication, and repair shop.

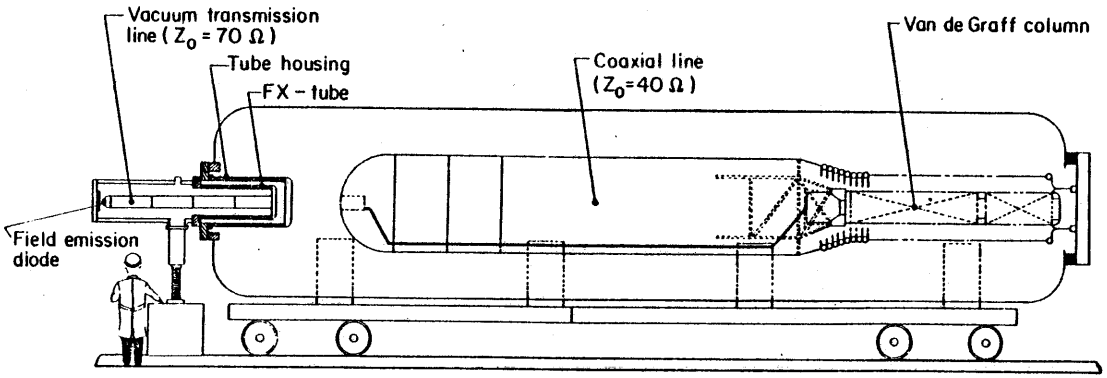

FIGURE 3.8-1. TREF FX-100 SUPER FLASH X-RAY MACHINE

Notes: Overall length, 60 ft.
Overall diameter, 12 ft.

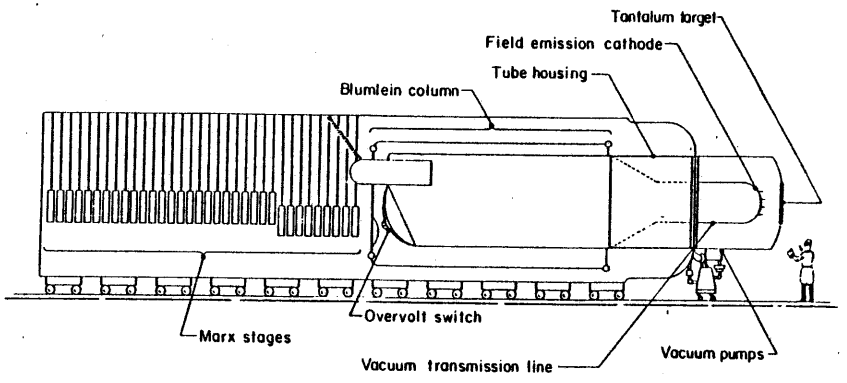

FIGURE 3.8-2. TREF MODEL 1590 SUPER FLASH X-RAY MACHINE

Notes: Overall length, 85 ft.
Overall diameter, 16 ft.

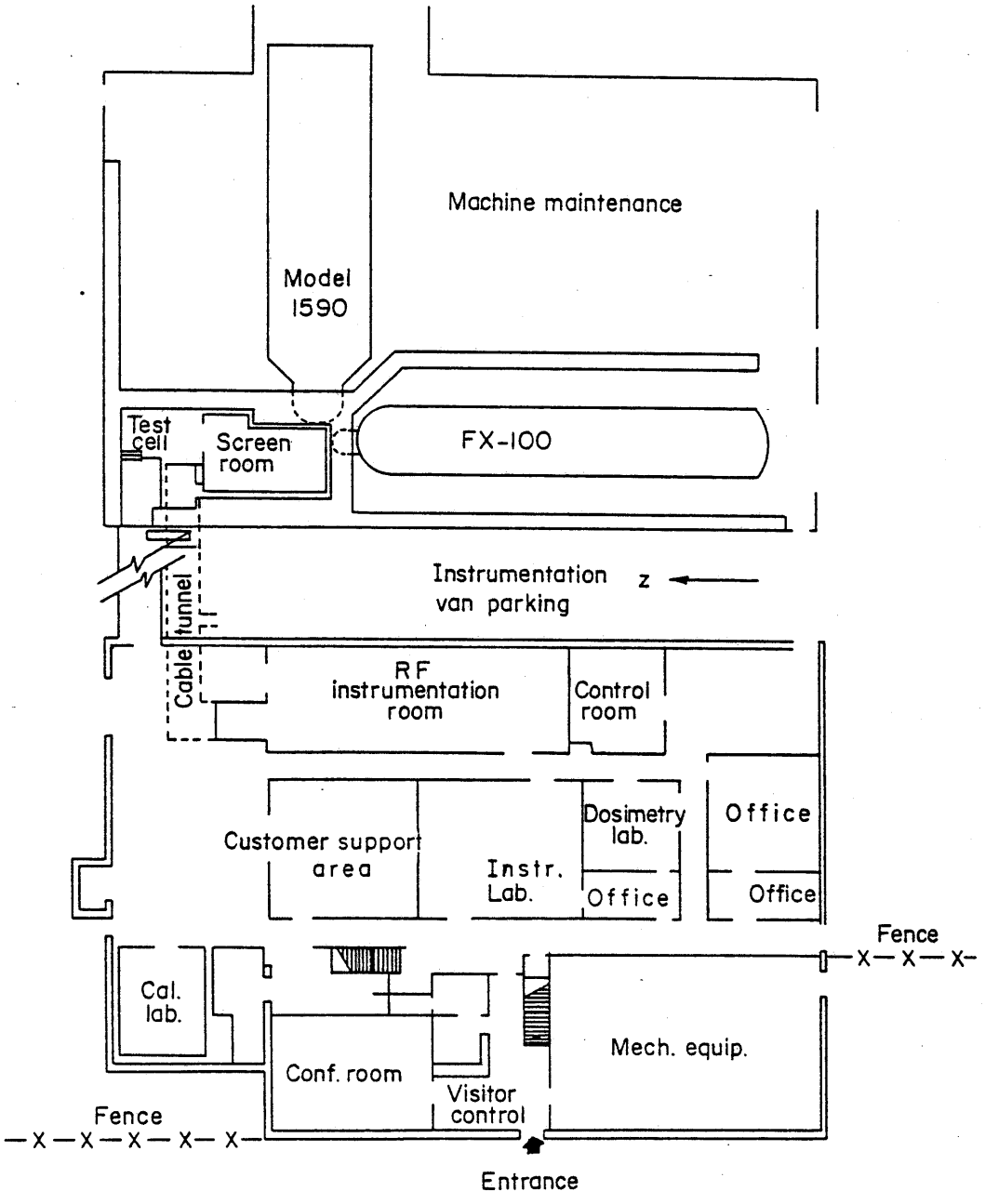

FIGURE 3.8-3. AFWL TRANSIENT RADIATION EFFECTS FACILITY FLOOR PLAN

TEST PARAMETERS

The two machines have been operated exclusively in the X-ray mode. Data only for this configuration are given in this report.

Operating Characteristics

Operating characteristics of the PULSERAD Model 1590 AFWL machine is given in Table 3.8-1.

TABLE 3.8-1. TREF FLASH X-RAY OPERATING CHARACTERISTICS(a)

	PULSERAD Model 1590
Maximum Output Voltage	10 MV
Bremsstrahlung Pulse Width (FWHM)	65 ns
System Stored Energy	500 kJ
Maximum Dose/Pulse at 75 cm	5000 rads(Si)

(a) Data are meant only to be used as a guide.

Total Beam Energy

Quantitative data are not available.

Beam Geometry

Beam has cylindrical geometry about its axis with a half-angle of 45 degrees (see Figure 3.8-4).

Repetition Rate and Pulse Predictability

The maximum repetition rate for the PULSERAD 1590 machine is 6 shots/h limited to 10 to 20 shots per day depending upon output levels.

The experimenter should be aware that the fidelity of a given pulse is not guaranteed and that sufficient diagnostics should be employed to monitor each shot. Typically ±10 percent of the predicted centerline dose is attainable for more than half the shots. There is some spot wander, as much as one inch, noticeable only on a close-in test.

Pulse Delay and Timing Jitter

Pulse delay is nominally 6 μs. This delay is defined as the time interval between the leading edge of the command pulse to the leading edge of the radiation output pulse.

Typically, jitter is less than ± 0.5 μs.

Electrical Noise

The primary difficulty in obtaining data at the facility is associated with the noise generated by the flash X-ray machines and the radiation environment. The noise is effectively eliminated by the blockhouse construction of the test cell and the use of the doubly isolated screen room on the Model 1590 only. Of greater concern to the experimenter are the electric and magnetic fields generated by secondary electrons knocked out of the test specimen and test cell walls, and the replacement current that neutralizes the net positive charge left on the test specimen by the escaping secondary electrons. This replacement current flows to the test package through the ground connections, inducing noise signals. The electrons flowing through the atmosphere surrounding the test package generate electric and magnetic fields in the test room which may induce noise signals in test leads. The signals exist only until the net charge is neutralized or the secondary electrons are absorbed in the test cell walls. This takes approximately 1.5 μs. The magnitude of the signals is directly dependent upon the experimental instrumentation, particularly on the grounding and isolation schemes. If the duration of the noise signals is not negligibly short, relative to the experimental data, or if they can cause irreversible or catastrophic effects, steps must be taken to eliminate them. Electromagnetic fields up to 1000 V/m may exist typically during the first μs, depending upon the mass of the test item.

Due to the significant dependence of noise signals upon test package configuration, no quantitative data regarding electrical noise are available. It is recommended that noise measurements and precautionary steps be taken during each experimental program. By careful test design, noise background on system test signal lines has been observed to be less than 10 mV (50 ohm).

Diagnostic Techniques

Radiation environment measurements are made by active and passive diagnostic systems. The active system utilizes two detectors in each of the radiation beams. The output from one detector is displayed on an oscilloscope.

The passive system consists of CaF_2 TLD's which are calibrated monthly against a cobalt-60 source.

APPENDIX B

SANDIA PULSED REACTOR DESCRIPTION
(from Ref. 13)

2.5 SANDIA PULSE REACTOR (SPR-II)

Sandia Laboratories
Albuquerque, New Mexico

CHARACTERISTICS

SPR-II is an all-metal, unreflected, and unmoderated critical assembly in the form of a right circular cylinder, 8 in. in diameter and 8.2 in. high. The assembly contains a total mass of 105 kg of fully enriched (93.2 percent U-235) uranium, alloyed with 10 weight percent molybdenum. A 1.5-in.-diameter "glory hole" extends vertically through the center of the core thereby facilitating internal as well as external irradiation of small test samples. It is at the mid-plane of the glory hole that the principal performance criterion, 1×10^{15} n/cm^2 (E > 10 keV*) per burst, is defined.

A thin-walled aluminum shroud approximately 8.75 in. square and 17 in. high covers the fuel assembly. The shroud, coated with boron, serves a dual purpose in ducting forced cooling gas over the fuel system by achieving relatively efficient cooling as well as diminishing the reactivity contribution of moderating test samples placed external to the reactor. Cooling reduces the maximum delay time between bursts to 2h.

The reactor is capable of operating in either the pulse mode or at a steady-state power of up to 3.0 kW for several hours. Steady-state operation is discouraged, however, because it produces large fission product inventories in the core.

Figure 2.5-1 is a cutaway view of the SPR-II fuel assembly.

Characterizing data presented herein are taken from detailed quantitative data obtained by Sandia Laboratories in a comprehensive effort to fully characterize the output and environment generated by SPR-II. Full appreciation is given in the Sandia data to experimental techniques, accuracy of the measurements, and the resulting uncertainties. A more thorough description of the reactor environment is available from the Sandia Laboratories through the references cited at the end of this section.

*Neutron energy spectrum will not be specified in the remainder of this section.

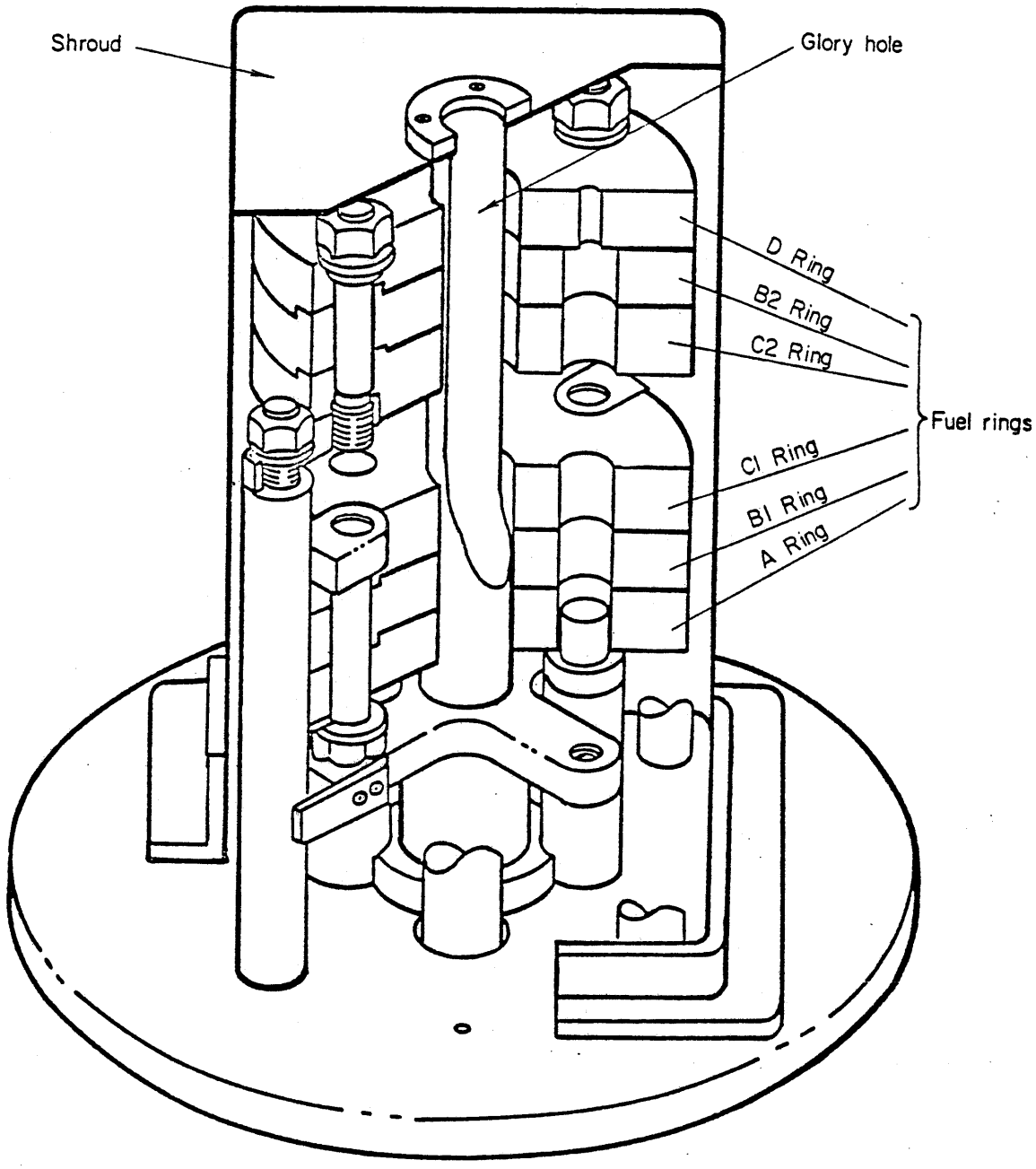

FIGURE 2.5-1. CUTAWAY VIEW OF SPR-II FUEL SYSTEM

TEST PARAMETERS

Operating Characteristics

Power Level

Burst power level is characterized by the temperature rise in the fuel. A standard SPR-II burst produces about a 350-400 C temperature rise (maximum). Measured characteristics for a 300 C burst are given in Tables 2.5-1 and 2.5-2.

Pulse Width and Initial Reactor Period

Pulse width varies inversely with burst size; the larger the temperature excursion the narrower the pulse. Figure 2.5-2 shows the relationship between pulse width and pulse yield. Figure 2.5-3 depicts three different burst profiles as measured with a photodiode.

Temperature-Time Profile and Characteristics

Cooling time (forced nitrogen) is 1 h.

Tolerable Reactivity Worth of Experimental Samples

Measured data regarding the tolerable reactivity worth of experimental samples indicate the following:

(1) The protective shroud around the fuel material isolates the reactor neutronically from experiments placed external to the core.

(2) Samples placed within the glory hole are very strongly coupled to the reactor. Measurements have been made regarding the reactivity worth of various sample materials in this position.

An assessment of sample reactivity worth will be made by the reactor staff for each experiment conducted.

Reactivity Insertion Rate

Reactivity insertion rate is \$10/s (max).

TABLE 2.5-1. NEUTRON FLUENCES[6]

Location	Operation	Neutron Fluence[a], > 10 keV
GH	Burst[b]	6.10×10^{14}
GH	Power Run 1 (PR1)[c]	6.36×10^{14}
GH	Power Run 2 (PR2)[d]	6.41×10^{14}
0" from shroud	Burst	1.25×10^{14}
0"	PR1	1.32×10^{14}
0"	PR2	1.31×10^{14}
6"	Burst	2.01×10^{13}
6"	PR1	1.95×10^{13}
6"	PR2	2.02×10^{13}
12"	Burst	8.13×10^{12}
12"	PR1	7.8×10^{12}
12"	PR2	8.17×10^{12}

(a) Fluences for PR1 operation have been multiplied by 3.0 for ease of comparison.
(b) 300 C ΔT burst.
(c) 18 kW-min power run.
(d) 54 kW-min power run.

TABLE 2.5-2. GAMMA DOSE[a], RADS (H_2O)[6]

Location	Operation	TLD 200 (CaF_2 - Mn)	TLD 100 Li F	Silver Phosphate
GH	Burst[b]	1.46×10^5	(1.134×10^5)[e]	1.61×10^5[f]
GH	Power Run 1 (PR1)[c]	2.06×10^5	2.34×10^5	2.14×10^5
GH	Power Run 2 (PR2)[d]	(1.58×10^5)[e]	2.35×10^5	2.36×10^5
0" from shroud	Burst	1.92×10^4	2.13×10^4	1.77×10^4
0"	PR1	2.36×10^4	3.08×10^4	1.97×10^4
0"	PR2	2.66×10^4	3.21×10^4	2.43×10^4
6"	Burst	3.12×10^3	5.28×10^3	--
6"	PR1	3.50×10^3	6.28×10^3	--
6"	PR2	4.01×10^3	6.38×10^3	--
12"	Burst	1.34×10^3	(5.02×10^3)[e]	--
12"	PR1	1.49×10^3	3.89×10^3	--
12"	PR2	1.53×10^3	3.96×10^3	--

(a) Doses for PR1 have been multiplied by 3.0 for ease of comparison. For more information on these tables see the section on the n/γ ratio.
(b) 300 C ΔT burst.
(c) 18 kW-min power run.
(d) 54 kW-min power run.
(e) Inconsistent with other data.
(f) Corresponds to 1-MeV gamma fluence of 3.24×10^{14} γ's/cm^2.

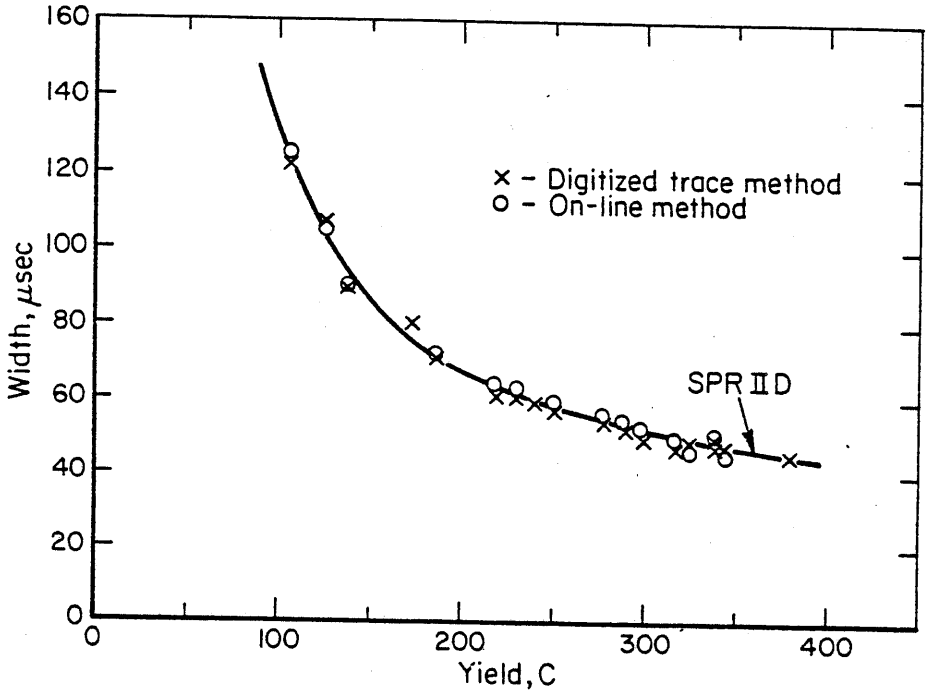

FIGURE 2.5-2. BURST WIDTH VS BURST YIELD

Yield is measured temperature rise.

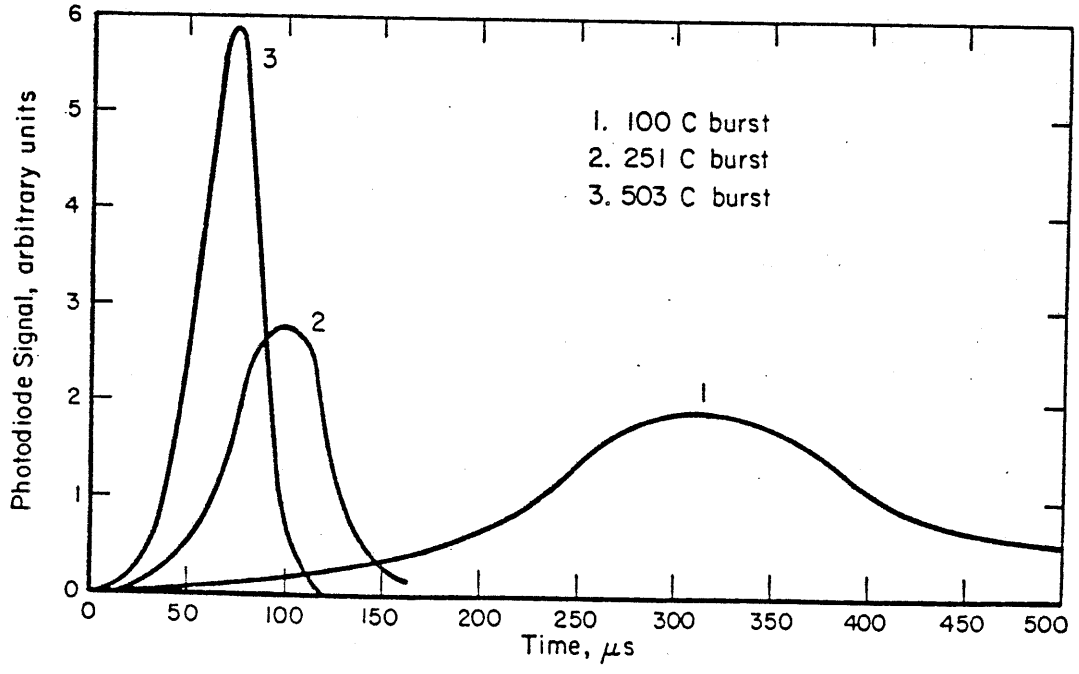

FIGURE 2.5-3. SPR-II BURST TIME PROFILES FOR VARIOUS-SIZE BURSTS AS DETERMINED WITH A PHOTODIODE